1ST YEAR REPORT

'Monomolecular silane coatings on magnesium/aluminium fuels'

by

David Quinn

July 1991

CONTENTS

CONTENTS (continued)

ACKNOWLEDGEMENTS

I would firstly like to thank Dr. S.Affrossman and Jim Queay for their aid and assistance on my project.

Secondly, special thanks goes to Chris McNab, Paul Menan, Jim Morrow and David Robb for their time, patience, and help which each has given me. Each has given me a taste of their infinite wisdom on their own chemistry and special thanks goes to them for sharing it with me.

Finally, thanks goes to the Royal Armanent Research and Development Establishment, Seven Oaks, Kent for funding the project and also for funding me throughout my first 12 months of the project.

Thank you one and all.

SUMMARY

The aim of this project was to investigate the curing reaction between CTBN and magnesium/aluminium alloy surfaces. A dispersion of magnesiun metal in this polymer produces a large increase in the viscosity of the dispersion with time. The chemistry occuring between the magnesium surface and the acid end groups of this particular polymer has been the subject of a previous study by McNab et al.

The previous involved coating the magnesium surface with an inert barrier to reduce the interactions with the acid groups of the polymer, and reduce particle/particle interactions. This project also dealt with chemisorbing silanes on to the surface, investigating the adsorption of particular silane compounds on the magnesium surface and performing rheological experiments with these coated magnesium particles and CTBN.

Surface analysis of the alloys show a high percentage of magnesium present on the surface of each alloy. Depth profiles indicate that when etching further into the alloy higher amounts of aluminium are exposed. Rheological analysis of these alloys dispersed 40% w/w in CTBN show increasing rates of change in viscosity with time for each alloy with increasing nominal amounts of magnesium. These results possibly indicate that the amount of aluminium present on the surface is related to the reaction rate in some way. The presence of aluminium in these alloys either thwarts the interaction of the magnesium surface with the acid end groups of the polymer, or is involved in a more complex manner.

INTRODUCTION AND BACKGROUND

A familiar property of magnesium metal is that once ignited magnesium burns fiercely producing a large output of energy, which has a high optical component. Because of this property in mind, magnesium has found its way into the world of pyrotechnics. Pyrotechnics are more commonly known as fireworks. Pyrotechnics are not just manufactured for our enjoyment on such occasions as military tatoos, bonfire nights or other means of celebration. Nowadays, pyrotechnics have become very diverse and sophisticated in both design and application in order to fulfil many essential military needs under a wide variety of operating conditions. Some of the many uses of pyrotechnics are shown in table 1.

Table 1. Some of the principal uses of Pyrotechnics

PYROTECHNICS	Light	Illuminants.	Flares and flashes.
		Signals.	Tracking and warning flares.
	Heat	Incendiary.	Napalm bombs, flame-throwers.
		Igniters.	Igniters for rocket propull.
	Smoke	Signal.	Coloured shell-bursts.
		Screening.	Smoke-shells and generators.
	Time	Delays.	Gas producing and gasless.

The ingredients of pyrotechnics are essentially intimate mixtures of finely powdered combustible substances (e.g. magnesium metal) and oxidants which, when suitably ignited, explode violently or burn steadily as required. The choice of fuels is very wide, ranging from metallic and non-metallic elements on the one hand to all manner of carbon-containing materials, both natural and synthetic, on the other.

The project involves research into the manufacturing aspect of pyrotechnics. Initially, pyrotechnics were mixed by hand-

sieving. This method was used for many years in mixing the less sensitive illuminating, signal and smoke compositions in quantities up to 3 or 4lbs in weight. The mesh of the sieve was adjusted to the size of the particles and the ease of which they flowed through the mesh. Safety precautions were also taken in order to protect the operator. All hand-sieving operations were carried out behind safety screens and also the sieve was earthed to stop the accumulation of static electricity.

Today, the manufacturing of plastic bonded pyrotechnics (plastic bonded pyrotechnics are pyrotechnics which are manufactured with a polymer to bind all the components together) is by extrusion of a fuel/oxidant/polymer mixture. The polymer binds the solid components, in the case of this project, magnesium metal as the fuel and potassium nitrate as the oxidant. The polymer used in the extrusion is CTBN (carboxy terminated butadiene acryonitrile) HYCAR grade 1300*13. CTBN is chosen as it produces a low amount of energy when cured with the other components. This gives the operator a much more safer material to handle instead of a possible igniting mixture. The polymer has a molecular weight of 570 000 and has the structure:

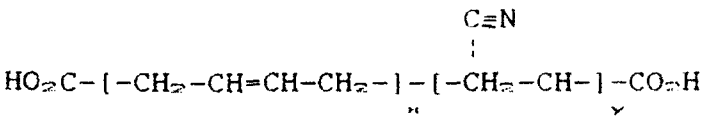

The pyrotechnic material also contains several other

components as well as the three main ones previously mentioned. The mixture also contains a chromium octanoate catalyst, and an epoxide curing agent (LY568) which has the structure:

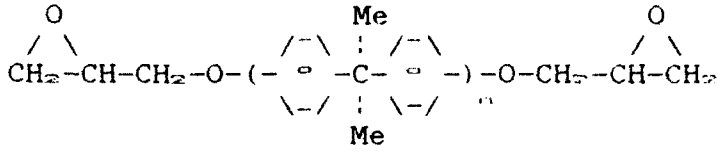

The plasticiser used in this mixture is:

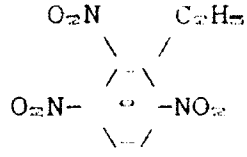

Extrusion is the blending together of materials in the molten state (the exception being metal powders). As mentioned previously, this is the method by which plastic bonded pyrotechnics are manufactured.

Primarily, the viscosity of this particular fluid will increase by the addition of solid particles. In the simplest case, the viscosity of filled liquids is described by the Einstein equation.

$$\eta = \eta_1 (1 + k_E \phi_2)$$

where, η = viscosity of mixture
η_1 = viscosity of suspending fluid
k_E = Einstein coefficient
ϕ_2 = volume fraction of filler

The actual value of k depends on the shape and orientation to an applied stress of the dispersed particles. (k_E=0.25 for spherical particles).

In practise, the viscosity of the dispersion will depend strongly on two different types of interactions. Firstly a particle/particle (e.g. magnesium/magnesium) interactions and particle/polymer (e.g. magnesium/CTBN) interactions. The particle/particle interactions will be a function of the size, shape and chemistry of the particular particles, and can lead to structuring of the metal filler in the mixture causing large increases in viscosity i.e. the solid can structure unevenly to produce a local laddering. The high loading of particulate matter with which this project is concerned exacerbates this effect.

Particle/polymer interactions can also occur in the mixture again causing structuring in the material. A reaction can occur between the terminal carboxylic acid end groups of the polymer and the filler surface (e.g. magnesium powder), causing a network to be formed throughout the dispersion.

Coating the solid surface with an inert barrier will protect the fuel from these two main sources of viscosity increase. Silane coupling agents have for this purpose been shown to be quite successful as inert barriers. Coupling agents are used both to increase interactions between a filler and a polymer for improvement of the mechanical properties of the composite material, and to decrease such interactions as in this case. At low concentrations, silane coupling agents give rise to significant improvements in mechanical and rheological properties. The purpose of the silane coupling agents in this project would be to protect the filler surface from the polymer, and by virtue of its lubrication effects decrease particle/particle interactions.

Examples of the silane coupling agents that are most widely applied to inorganic fillers include aminopropyl' iethoxysilane, (APS) [1,2], and

methacryloxypropyltrimethoxysilane, (MPS) [3,4].

The method by which these silane coatings are applied to filler surfaces involves the pre-hydroylsis of the alkoxy functions to form hydroxyl groups. The material then deposits as a polysiloxane coating;

$$R\text{-}Si(OR)_3 \longrightarrow R\text{-}Si(OH)_3 \longrightarrow -Si\text{-}O\text{-}\underset{\displaystyle O}{\overset{\displaystyle R}{Si}}\text{-}O\text{-}Si$$

The siloxane encapsulates the metal filler by deposition of oligomers and small chains on to the metal surface, these then undergo further polymerisation to produce a complete overlayer. The stability of the coating is enhanced by crosslinking of the siloxane chains.

The siloxane coating formed on adsorption of trifunctional hydroxy silanes on magnesium contributes nothing to the performance of the pyrotechnic, so ideally the coating should be as thin as possible. It is difficult to ensure even distribution of a very thin siloxane coating on a manufacturing scale, since a solution of the coupling agent must be stirred with a slurry of the filler while the solvent is evaporated off. This would lead to a situation in which some areas of the filler will have thicker layers of coupling agents than in others.

A possible technique for the deposition of silanes on to the magnesium surface, giving a much more even distribution around the surface, would be to utilise direct chemical bonding of molecules containing silyl functions on to the surface i.e. chemisorption of silanes on to the magnesium surface.

Work has been carried out on the chemistry of

chemisorbing silanes on to magnesium oxide surfaces by M^{c}Nab and others [5,6]. M^{c}Nab synthesised a number of selected organic compounds with silane functionalities with the view to chemisorbing them onto magnesium oxide. These coated particles were dispersed 8% w/w in CTBN 1300*15 and their rheological results obtained. The polymer used experimentally is a factor of 10 less in molecular weight than the one used commercially, thus enabling a higher level of filler loading, which increases interfacial reactions, and, hence a better understanding of the chemistry of the reaction. M^{c}Nab performed most of his adsorption studies on magnesium oxide powder. This has a higher surface area than that of magnesium metal (Mg = $0.2m^{2}g^{-1}$: MgO = $10m^{2}g^{-1}$). The higher surface area of magnesium oxide facilitates better adsorption studies than that of magnesium powder. M^{c}Nab extenisively used DRIFTS (Diffuse Reflectance Infrared Fourier Transform Spectroscopy) to investigate the bonding of the silanes on the magnesia surface. Rheology experiments were conducted on a Carri-med Controlled Stress Rheometer (CSR).

Research is now being carried out on a series of magnesium/aluminium alloys (another fuel component). Each alloy has a different percentage content of magnesium. The research is following the same guidelines as set out by M^{c}Nab and others [5,6]. Results from the adsorption and rheology studies will be quite interesting as we have little idea about how the presence of aluminium will affect chemistries when compared to magnesium alone.

Some results have been obtained for these alloys and these will be discussed later in this report.

CHAPTER 1 : THE SURFACES OF MAGNESIUM AND ALUMINIUM

This project involves the investigation of the interaction between the filler surface and the carboxylic acid end groups of the polymer. The nature of the surface of the metal filler is obviously of prime importance.

1.1 Magnesium

Magnesium is a reactive metal and reacts readily in air to form an oxide overlayer. The oxide content of magnesium metal is typically 1-2%. Since the surface area of the metal powders is of the order of $0.2 m^2 g^{-1}$, it can be expected that the oxide overlayer is relatively thick, and that the chemistry of the metal surface will be similar to that of the magnesium oxide surface.

Magnesium oxide surfaces have been studied mainly in the context of catalytic reactions, where it is used either as a support [7,8] or as a catalyst in its own right. It has been found to catalyse, for example, the isomerisation of alkenes [9], and the conversion of benzaldehyde into benzyl benzoate [10,11]. Other studies involving adsorption on to magnesium oxide surfaces have involved ethanol [12], and formaldehyde [13].

The adsorption properties of magnesium oxide are due to its surface basic properties and depend largely upon the amount of preadsorbed carbon dioxide. The adsorption of carbon dioxide onto magenesium oxide has been used to characterise the basic properties of its surface.

Carbon dioxide adsorbs onto magnesium oxide in three stages [14]. Firstly, a rapid physical adsorption, secondly, a slow chemisorption involving the formation of a bidentate carbonate ion, and finally, a still slower chemisorption resulting in the formation of a carbonate ion similar to that found in bulk

magnesium carbonate. In addition, water (H_2O) dissociatively chemisorbs onto magnesium oxide to form protons and hydroxyl ions, this indicates the highly polar nature of the magnesium oxide surface.

The surface of magnesium oxide can have both basic and acidic sites existing simultaneously. The stronger acid sites are only developed after treatment at high temperatures, so under the conditions expected in our work the surface of the oxide will display mainly basic properties.

The basic sites have been classified into three different types [15]. Firstly, strongly basic O^{2-} ions which on exposure to CO_2 are transformed to CO_3^{2-} ions. Secondly, strongly basic centres derived from the O^{2-} ions adjacent to the surface OH groups, and finally, the surface OH groups themselves. The OH groups on the surface have been shown to be uninvolved in CO_2 adsorption, since samples of MgO heated to remove the OH groups from the surface adsorb the same amount of CO_2 as unheated samples [15]. Work carried out by Affrossman and others at the university of Strathclyde have also indicated that the OH groups present on the magnesium oxide surface play no part in the reaction between the acid end groups of the polymer and the magnesium oxide surface. It shows that the acid end groups of the polymer seem only to react with other particular basic sites also present on the surface.

Of the three types of basic sites present on the magnesium oxide surface mentioned above, it has been found that the O^{2-} ions adjacent to the surface OH groups can assist in the formation of anions from adsorbed species containing labile hydrogen by abstraction of a proton to form a surface OH group

[16]. If we take for example the adsorption of formaldehyde onto MgO, this results in the abstraction of a proton to form a formate anion HCO_2^-. At low temperatures (170K) the adsorbed formaldehyde is converted to polyoxymethylene ($[OCH_2]_n$). This polymerisation is catalysed by the same basic sites as the formaldehyde to formate reaction [13]. The O^{2-} sites have also been shown to be involved in the formation of ethoxide ions from ethanol. The participation of Mg^{2+} ions acting as Lewis acid sites in this process has been proposed [12].

Another possible active site on the MgO surface is the O_2^- ion. This has been found to form on MgO following the adsorption of pyridine [17]. The formation of organic anions such as trinitrobenzene following adsorption onto the MgO surface has also been presented as evidence for the formation of O_2^- but direct electron transfer from O^{2-} ions in low co-ordination sites to the adsorbed species. Published work on the O_2^- ion deals mainly with clean MgO surfaces examined under carefully controlled conditions. The O_2^- ion is reactive in the presence of polar molecules such as H_2O. On exposure to atmospheric moisture, the concentration of O_2^- ions (detected by ESR) on the surface rapidly decreases [18].

1.2 Aluminium

Aluminium is another reactive metal which reacts readily with the oxygen present in the atmosphere to produce an oxide overlayer. It can therefore be expected that the chemistries of the oxide overlayer on aluminium powder to be similar to that of pure aluminium oxide (alumina). Alumina has a far greater surface area than that of magnesium oxide (MgO = $10 m^2 g^{-1}$: Al_2O_3 = $100 m^2 g^{-1}$). The larger increase in surface area makes alumina a far more attractive material for adsorption studies.

The first major study of the alumina surface was carried out by Peri and Hannan [19] in 1960. Peri and Hannan were able to prepare a highly transparent porous plate of g-Al_2O_3 and investigate the spectra of several samples in the 4000 to 1500cm^{-1} region. For an undried sample, bands near 3300 and 1650cm^{-1} were observed and, in accordance with prior spectroscopic data on silica gel, these were assigned to the stretching and bending frequencies of molecular water adsorbed on the alumina surface. Evacuation at 400°C caused desorption of the bulk water, and the resultant spectrum showed the presence of several distinct bands in the 3700cm^{-1} region. After evacuation at 700°C the spectrum was well defined, three peaks being observed at 3698, 3737, and 3795cm^{-1}. These bands are essentially symmetric and are assigned to the stretching vibrations of isolated surface hydroxyl groups.

On heating to 850°C, the surface hydroxyl groups are slowly removed. The rate of removal of these OH groups at high temperatures, however, is not identical, and it was observed that the intensity of the band at 2759cm^{-1} (= 3737cm^{-1}) was reduced more rapidly than that of the other two bands. This independent behaviour of the surface hydroxyl groups was also observed by Peri and Hannan during isotopic exchange of the surface hydroxyl groups with deuterium and in the reaction of butene with a deuterated sample. In the first case, when deuterium gas was added to the alumina surface between 250°C and 500°C, the central OH band changed in intensity more slowly than the other two bands and is thus the least susceptible to this exchange reaction. The hydroxyl group responsible for the lowest frequency change hydroxyl vibration was able to exchange its H for D faster than the other two groups, and since this low frequency band was the only one to

undergo an exchange reaction when butene was added to the completed deuterated surface. this can be taken as an indication that this hydroxyl group is the most acidic of the three types that exist on the alumina surface.

Peri and Hannan used the exchange reaction between deuterium gas and surface aluminol groups to determine the number of such groups present on their sample. The average absorptivity of the isolated OH groups was calculated to be about $8*10^4 cm^2$/mole. Readsorption of water at room temperature on to a sample of alumina that had been baked at 800°C gave rise to a spectrum characteristic only of absorbed water. No increase in the number of surface hydroxyl groups was noted unless the water and alumina were heated together at 300°C. at which temperature preferential formation of the highest frequency ($3698 cm^{-1}$) OH group was observed. During the adsorption process, only one of the surface hydoxyl bands (at $3795 cm^{-1}$) was perturbed by the water adsorption.

Peri also reported on the spectrum of alumina recorded at temperatures up to 800°C. At 800°C. all bands were broadened and moved to lower wavelengths, the displacement being about $30 cm^{-1}$. However, even at this temperature. the bands were distinct, indicating that the surface hydroxyl groups are not in random motion but are localised on distinct surface sites. With this particular sample of alumina. additional surface hydroxyl groups were identified at 3780 and $3733 cm^{-1}$.

The presence of these five types of hydroxyl groups has been explained by Peri [20] on the basis of a computer model of the alumina surface. This model is obtained by considering the dehydration of a fully hydroxylated. 1 0 0 crystal face of alumina. A square lattice. initially filled with hydroxyl ions.

was assumed (Fig.1), and four arbitary rules were established for the dehydration process.

Figure 1: Computer model of a dehydroxylated alumina surface; + denotes Al^{3+} in lower layer.

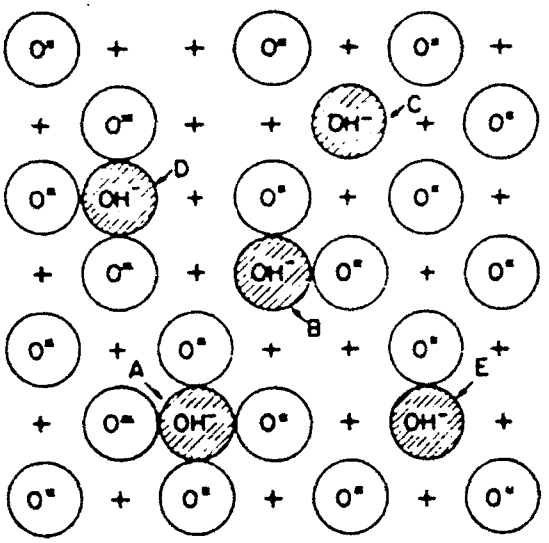

The resultant computer model predicted a surface containing five different types of hydroxyl groups. The assigned vibrational frequencis of these five different hydroxyl groups are shown in table 2.

Table 2. Hydroxyl Groups on Alumina*

Band	Wavenumber cm^{-1}	No. of nearest oxide neighbours
A	3800	4
B	3744	2
C	3700	0
D	3780	3
E	3733	1

* Assignment of frequencies by Peri [20] with reference to Fig.1.

CHAPTER 2 : EXPERIMENTAL TECHNIQUES

As the project is surface orientated it therefore requires modern surface techniques to analyse the surfaces of our substrate.

Three of the most useful methods which will be used extensively throughout the whole of this project to examine the surfaces will be Secondary Ion Mass Spectrometry (SIMS), Diffuse Reflectance Infrared Fourier Transform Spectrometry (DRIFTS) and X-ray Photoelectron Spectroscopy (XPS). Controlled Stress Rheometry (CSR) techniques are also utilised to investigate viscosities.

2.1 Secondary Ion Mass Spectrometry (SIMS)

Secondary Ion Mass Spectrometry (SIMS) has become a very powerful technique for studying the chemical state of solid surfaces.

SIMS is the mass spectrometry of atomic or molecular particles which are emitted when a solid surface is bombarded by energetic primary particles. This process of emission is known as 'sputtering'. The primary particles are commonly ions and the secondary ions that are emitted from the surface are either in the ionised state or initially as neutral particles, which are then ionised before analysis in the mass spectrometer. This phenomenon of sputtering can be showed more clearly in figure 2.

Figure 2: A diagram of the SIMS phenomenon indicating the collision of the primary particle with a solid surface and the emission of secondary particles.

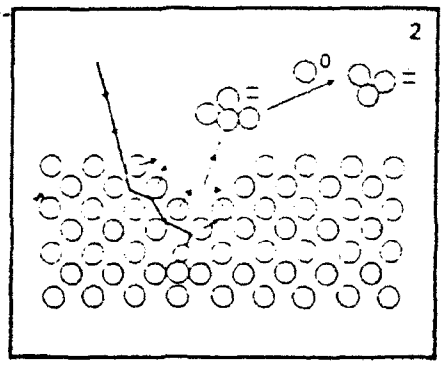

The SIMS experiment involves ion bombardment and detection of emitted ions. The experiment must therefore be conducted under high vacuum conditions. The equipment is usually constructed of stainless steel. The two main components of the experiment are the primary ion beam and the mass spectrometer. The specification and mode of each depends on the primary beam parameters being used.

There are three types of SIMS techniques in common use and each has different primary ion gun parameters. The first of these experiments is 'Static SIMS'. Static SIMS uses a low flux primary ion source. The primary beam currents are of $<10nAcm^{-2}$. These conditions yield surface monolayer lifetimes of many hours to several days. Static SIMS can be used for studying not only elemental composition but also the chemical structure of the surface.

The second technique is 'Dynamic SIMS'. This uses a high flux density of oxygen or caesium primary ions to obtain a very high yield of secondary ions. In this case the surface is eroded very rapidly to yield high sensitivity depth profiles.

Dynamic SIMS is almost exclusively used for elemental analysis.

The final SIMS technique is 'Imaging SIMS'. Imaging SIMS uses a recently developed microfocused liquid metal ion beam. By raster scanning the beam across an area of surface (i.e. moving the beam across the surface to draw out a square area, very like a television) and collecting the secondary ions at each point a chemical image can be obtained.

A table summarising the different experiments and the different conditions required for each is shown below in table 3.

Table 3: Primary beam parameters for each SIMS experiment

Analysis mode	Beam current	Surface lifetime
Dynamic SIMS	O_2^+ >10uAcm^{-2} Cs^+	<1s
Static SIMS	Ar^+ <10nAcm^{-2} Ar^0	>10^3s
Imaging SIMS	Ga^+ ca10nAcm^{-2} In^+	<10^3s

In common with many techniques of surface analysis that use a charged particle as the probe species there will be the possibility of surface charging. This results in spectral loss or instability especially when studying the surface of non-conducting materials. To overcome this the surface of the sample being analysed is flooded with low energy electrons. This decreases the surface charging enabling us to study insulating materials.

SIMS can be applied to all types of solid materials from catalysts to polymers to metal alloys.

2.2 Diffuse Reflectance Infrared Fourier Transform Spectroscopy (DRIFTS)

Diffuse Reflectance Infrared Fourier Transform Spectrometry (DRIFTS) is another technique which will be extensively used with this project.

When infrared radiation falls onto the surface of a sample it can be either absorbed and directly reflected by specular reflectance or diffusely scattered. These two cases are illustrated in figure 3.

Figure 3: Diagram of infrared radiation entering and leaving a solid sample in a DRIFTS experiment.

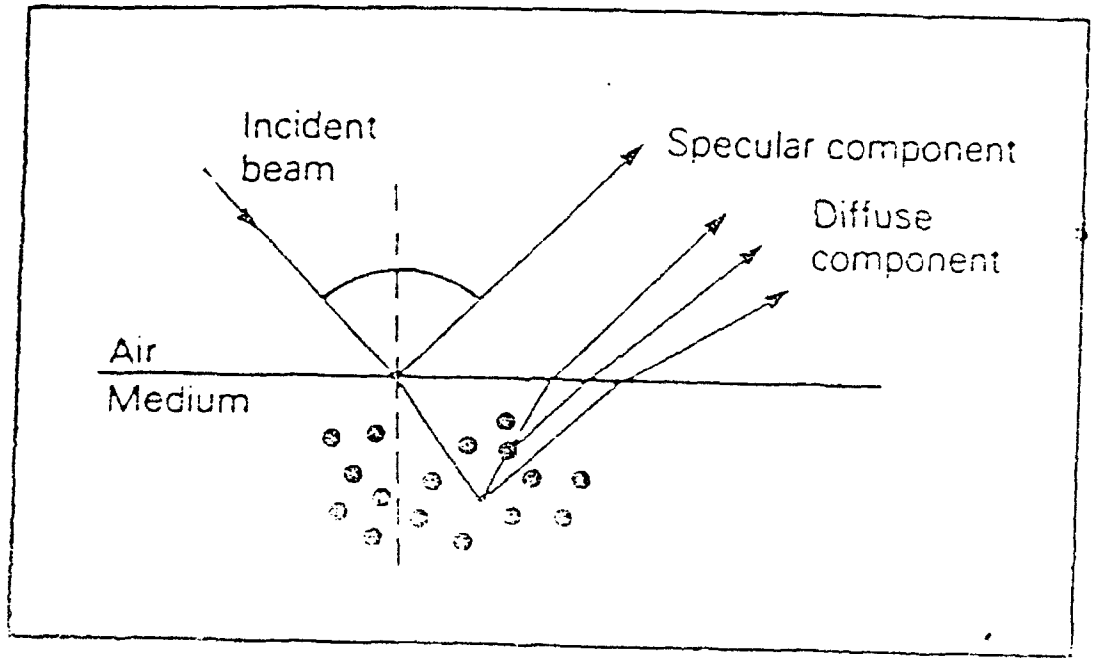

Diffuse reflectance is the study of the diffusely scattered component.

Figure 3 illustrates the scattering of radiation from the surface of a solid sample. If the surface is smooth then the radiation will be reflected back at a (finite angle. As the infrared radiation hits the sample surface some of the energy in the beam is adsorbed and the reflected radiation will contain spectral information unique to that particular sample. This form of reflection is known as 'specular reflectance' and there are many commercial devices on the market which can measure the specular reflectance. Specular reflectance is usually applied to samples that have reflective surfaces e.g. the insides of aluminium drinking cans.

When the radiation is not reflected back at any particular angle but is scattered over a wide area, this is known as 'diffuse reflectance'. Again, as with specular reflectance, as the infrared beam penetrates the sample surface selective adsorption of some of the wavelengths contained in the radiation will occur and the reflected radiation will contain spectral information unique to that sample. This technique has many more applications than specular reflectance as nearly all samples exhibit some sort of diffuse reflectance.

One essential piece of equipment which is essential to the DRIFTS experiment is the 'DRIFTS cell'. This is a cell with a sequence of mirrors in which the mirrors are adjusted to focus the maximum infrared radiation onto the sample and to focus the scattered infrared radiation into the detector thus increasing the signal/noise ratio giving a much more detailed spectra. Figure 4 illustrates the 'DRIFTS cell' and the purpose of the mirrors.

Figure 4: The 'DRIFTS cell' illustrating the path of the infrared radiation within the cell.

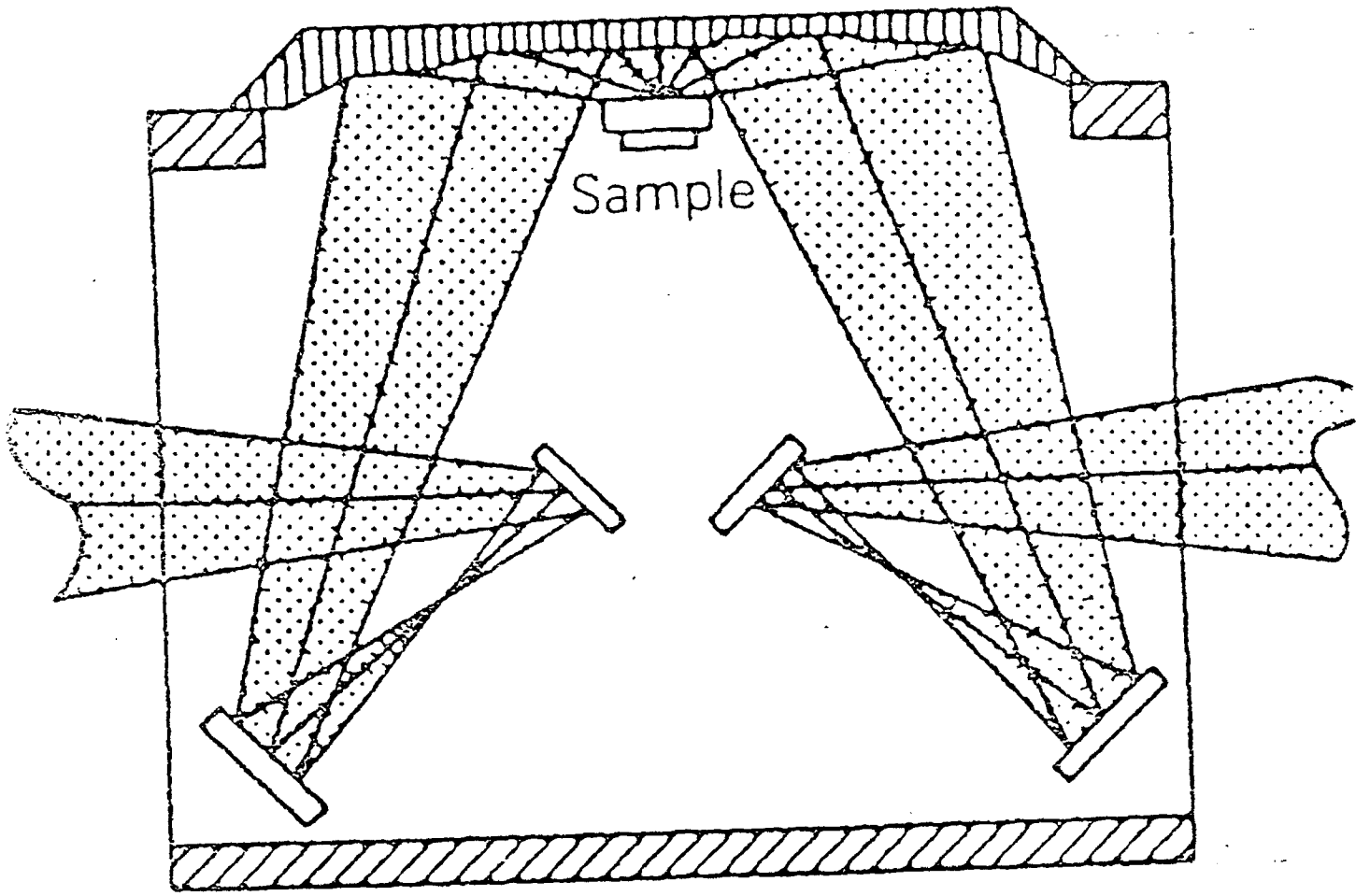

Diffuse reflectance can be used to analyse most samples. However, its main application is in the analysis of solids. One of its major advantages is that sample preparation time is significantly reduced. All that is needed to obtain a good quality spectrum from a sample is to spread the sample onto the surface of a layer of KBr powder. Alternatinvely, better quality results can be obtained by mixing the sample with KBr. This is the method by

which all DRIFTS spectra will be collected throughout this project. Another good advantage of this technique is that good quality spectra can be obtained for very small amounts of sample.

Using the FTIR spectrometer with the DRIFTS cell we are able to use a function of the spectrometer which enables the user to subtract spectra. The subtraction of a coated sample from an uncoated sample allows isolation of the spectra of the absorbed species on the substrate [21,22].

2.3 X-ray Photoelectron Spectroscopy (XPS)

X-ray photoelectron spectroscopy (XPS) is a surface analytical technique which was developed in the 50's and 60's by K.Seigbahn at Uppsala university in Sweden. As its name implies, XPS utilises x-rays (normally Al K_α and Mg K_α) to bombard a sample (gas, liquid or solid) causing ejection of electrons. The energies of the emitted electrons are measured in an energy analyser. Although inner core, valence and auger electrons are all emitted, XPS is used principally in determining the binding energy of the core level electrons. The kinetic energy of the emitted photoelectron is related to its binding energy by Einsteins relationship:

$$B.E. = h\nu - K.E. - \pounds \qquad \text{----- (1)}$$

where B.E. is the binding energy of an electron in a particular orbital, hv is the photon energy (Al K_α = 1486.7eV; Mg K_α = 1253.7eV) and £ is the work function minus the difference between the fermi-level and a free electron. For conducting samples the value of £ is that of the spectrometer material, $\pounds_{sm}$, which is constant. Hence equation (1) reduces to:

$$B.E. = Constant - K.E. \qquad \text{----- (2)}$$

By measuring the K.E. of the emitted photoelectrons B.E.s can be

determined, and as each B.E. is unique, elemental identification is possible. Small shifts in B.E. (chemical shifts) are also very important providing information on the chemical environment of the element(s) being studied.

When analysing non-conducting samples, analysis is not so straightforward as charging of the sample can occur (c.f. SIMS). This results in charge broadened peaks which are shifted in energy from their normal B.E. position. Several ways of overcoming this problem exist, but by far the most convenient method is to refer all peaks in the spectrum to that of adventitious carbon at 284.7eV (always present in oil vacuum systems) or some known sample peak.

XPS is a surface technique. The surface specificity arises because only those electrons which are emitted elastically contribute to the photoelectron peak; and these originate in the outermost atomic layers (~20-50Å). Other electrons which suffer energy losing collisions before they are emitted contribute to the bachground spectrum, therefore, a typical full scan spectrum consists of sharp photoelectron peaks superimposed on a sloping background.

Because of the nature of the technique (utilising x-rays: measuring electron energies and: high surface specificity) XPS experiments are carried out under high vacuum (10^{-9} - 10^{-10} Torr). The better the vacuum the less chance on contamination build up during the course of the experiment. Therefore, spectra obtained under good vacuum conditions are more likely to reflect the sample surface than those taken in a poor vacuum. The principal contaminants in vacuum systems are CO, H_2 and hydrocarbons, arising from the oils used in the vacuum pumps.

2.4 Controlled Stress Rheometry (CSR)

The project deals with measuring the rheology (viscosity) of metal fillers dispered in polymer. To measure this a Carri-med Controlled Stress Rheometer (CSR) is utilised.

Rheology is the measurement of the flow and deformation behaviour of materials. Controlled Stress Rheometry is a very versatile technique which can be used to characterise the properties of any sample which can be loaded into the instrument. This means that a very wide range of industrial and research materials can be measured. The properties of a material characterised by techniques such as flow curves, creep or oscillation can help to predict and control the behaviour of the material during manufacture, storage or use.

The Controlled Stress Rheometer (CSR) is versatile in the number of different rheological modes which it can carry out, and is therefore ideally suited to 'modelling' real situations.

The flow behaviour of a material is decribed by the relationship between the force acting on the sample of a material, and the effect of that force. The effect may be elastic deformation or viscous flow.

The advantage of using a controlled stress rheometer is that it can measure the effect on the sample of minute, non-destructive forces which can give invaluable information concerning the interactions inside the test material, as well as measuring the shear stress/ shear rate relationship at higher stresses, hence, the controlled stress technique can give a more complete analysis of the state of a test sample.

The controlled stress rheometer has different operating modes for different rheological analysis. The operational mode concerned with this project is the controlled stress flow mode.

This mode enables the user (once the sample is flowing) to measure the viscosity at a desired shear stress. This enables the instrument to simulate the conditions under which the material tested should have specific properties, such as suspensions

The operating conditions which are used for this project are shown in Fig.5.

Figure 5: Operating conditions for project.

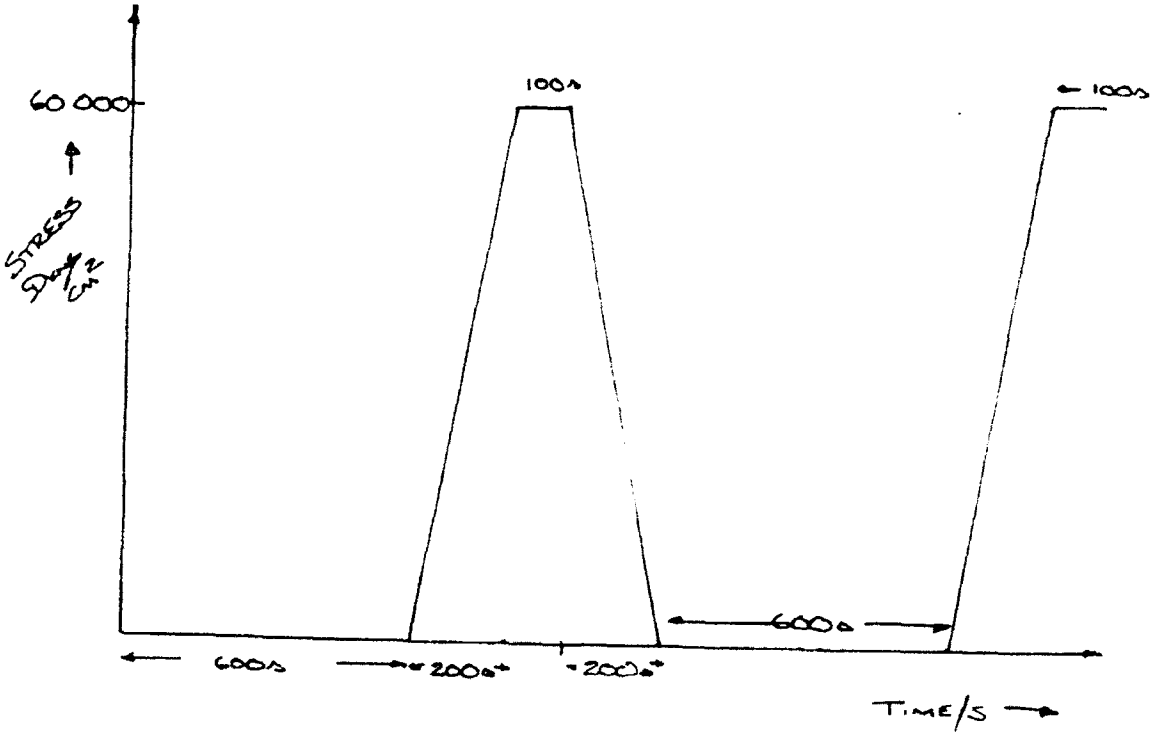

CHAPTER 3: RESULTS AND EXPERIMENTAL

The aim of this project was to study the adsorption of selected adsorbates on magnesium/aluminium alloys and to investigate the rheological properties of these coated magnesium/aluminium alloys.

3.1 Synthesis of adsorbates

Attempts were made to synthesise an alkyl-catechol derivative [23] for further adsorption studies on magnesium/aluminium alloy surfaces.

Two experimental procedures were applied in order to synthesise the catechol derivative. The first procedure is given below.

The first step was to prepare the crude acid chloride. 0.1 mole (11.9g) of thionyl chloride was placed in a 100ml round-bottomed flask. The flask was then placed in an oil-bath where then the temperature of the bath was raised to 40°C. At this temperature, 0.1 mole (11.6g) of hexanoic acid was dripped into the contents of the flask over a ten minute period. The temperature of the bath was then raised to 70°C and maintained at this temperature until no more hydrogen chloride and sulphur dioxide evolved (~1 hour). The reaction mixture was stoppered and allowed to stand overnight.

A 500ml round-bottomed flask equipped with a mechanical stirrer, dropping funnel and reflux condenser was assembled. 0.3 mole (39.9g) of anhydrous aluminium chloride, 0.1 mole (11g) of catechol and 100cm^3 of carbon bisulphide were put into the 500ml round-bottomed flask. The acid chloride prepared the day before was put into the dropping funnel. The mixture in the flask was stirred at room temperature for 15 minutes and then at 40°C (oil-

bath temperature) for one hour. After this, the crude acid chloride was then dripped in over a period of 10 minutes. The temperature of the oil-bath was raised to 70°C over a 10 minute period and kept at 55-60°C for one hour. During this time the carbon bisulphide evaporates (or distilled) off and the temperature of the oil-bath was raised to 140°C and maintained at this temperature for 4 hours.

The mixture was allowed to stand overnight and was decomposed by slowly adding 150cm³ of hydrochloric acid (75cm³ water: 75cm³ conc. hydrochloric acid). On cooling, the catechol derivative was extracted with n-butanol, and washed with water. The derivative is recovered by distillation: yield 14.5g of distillate, boiling at 220-225°C (5mm).

The second procedure applied to synthesise the catechol derivative involved placing 0.1 mole (11g) of catechol in a 500ml, three-necked, round-bottomed flask equipped with a dropping funnel, mechanical stirrer and reflux condenser. The flask was placed in an oil-bath and the temperature of the oil-bath was raised to 120°C to melt the catechol. At this temperature, while stirring, one mole of crude hexanoic chloride was dripped into the flask over a 20 minute period. Stirring was continued at this temperature until the evolution of hydrogen chloride ceased (~30 minutes). The product, substantially catechol diester, was allowed to cool.

The second step of the procedure was to place 0.5 moles (67g) of anhydrous aluminium chloride and 120cm³ of carbon bisulphide in a 500ml, three necked round-bottomed flask equipped with a reflux condenser, mechanical stirrer and dropping funnel. The mixture was stirred while a mixture of the diester and another 0.1 mole (11g) of catechol was slowly dripped in. Stirring

was continued at room temperature until the evolution of hydrogen chloride ceased, after which the flask was placed in an oil-bath and heated slowly to 80°C. After this, the dropping funnel is removed and a downward-distilling condenser is connected to allow the carbon bisulphide to be distilled off. The temperature of the oil-bath was then raised to 135°C and stirring was continued at this temperature until the reaction mass became too viscous. Heating was continued at this temperature for four and one-half hours. After cooling, the reaction mixture was decomposed by adding cautiosly 100cm^3 of hydrochloric acid (50cm^3 water: 50cm^3 conc. hydrochloric acid). The mixture was allowed to stand for 2 hours, to cool. The catechol derivative was then extracted with n-butanol, and washed with water. The derivative is recovered by distillation: yield 14.5g of distillate, boiling at 220-225°C (5mm).

The above procedures were attempted several times but all were unsuccessful.

3.2 Surface analysis of magnesium/aluminium alloys

When the alloys were obtained the first step was to determine the nature of the surface of each alloy using Secondary Ion Mass Spectrometry (SIMS). These experiments were carried out at the university of Ulster, Coleraine, Northern Ireland, with the assistance of Prof. N.Brown and C.Anderson in order to utilise their dynamic SIMS facility.

The experimental conditions for each alloy was that firstly a static SIMS scan was performed at "1000 zoom". This gathers information from a sputter etched rectangle of area ca. 3mm*2.5mm, which gave a spectra of the 'real surface' of each alloy. Secondly, depth profiles were obtained. These depth

profiles were recorded at "200 zoom". This gathers information from a sputter etched rectangle of area ca. 0.6mm*0.5mm. Finally, static SIMS was performed on the material exposed at the bottom of the etch pit (sub-surface) at "200 zoom". For each alloy a mass scan of the 'real' and 'sub' surface was obtained along with a sensitive depth profile. The results obtained from these experiments are shown in the following pages.

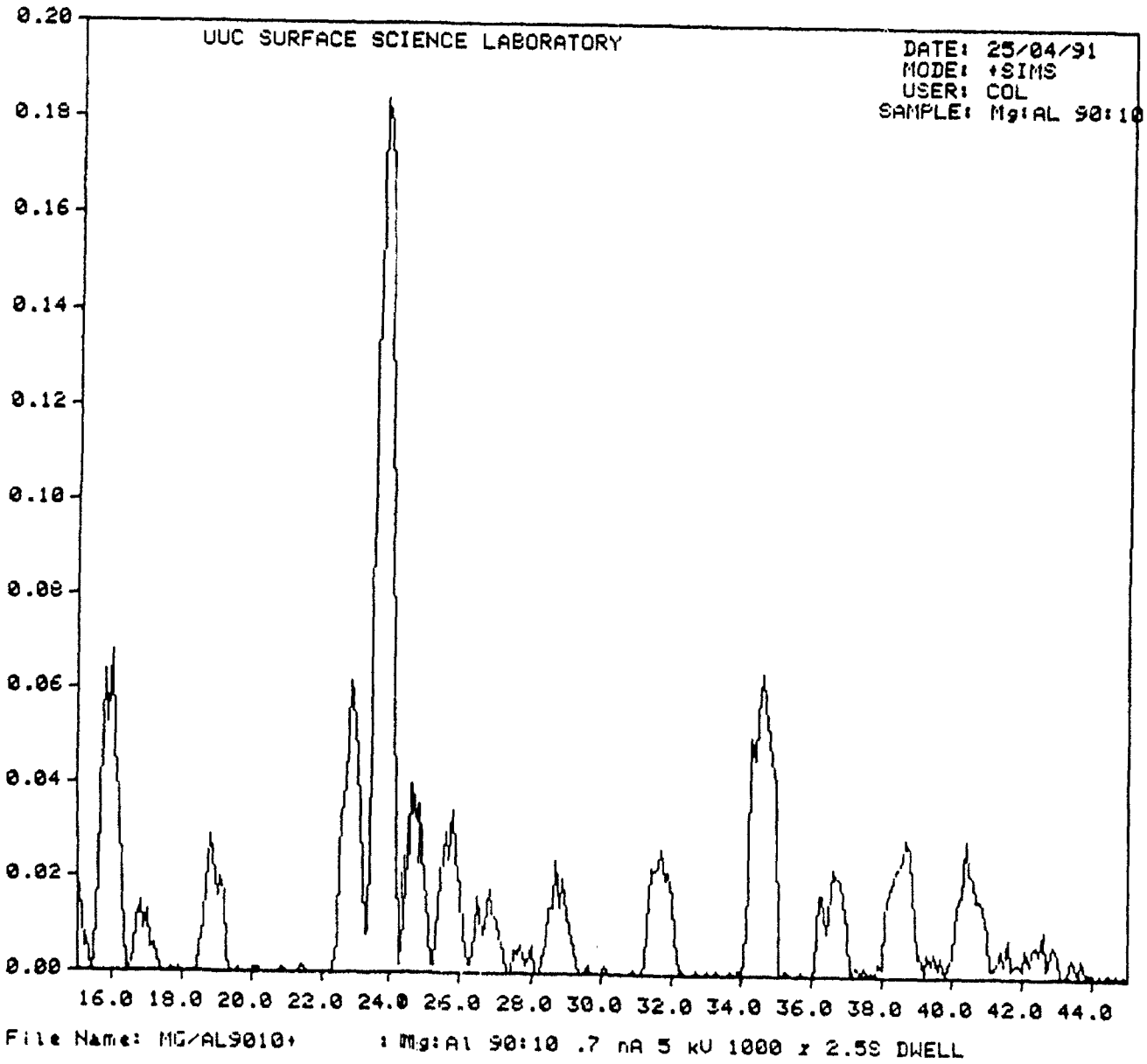
UUC SURFACE SCIENCE LABORATORY
DATE: 25/04/91
MODE: +SIMS
USER: COL
SAMPLE: Mg:AL 90:10
0.20
0.18
0.16
0.14
0.12
0.10
0.08
0.06
0.04
0.02
0.00
16.0 18.0 20.0 22.0 24.0 26.0 28.0 30.0 32.0 34.0 36.0 38.0 40.0 42.0 44.0
File Name: MG/AL9010+
: Mg:Al 90:10 .7 nA 5 kV 1000 x 2.5S DWELL

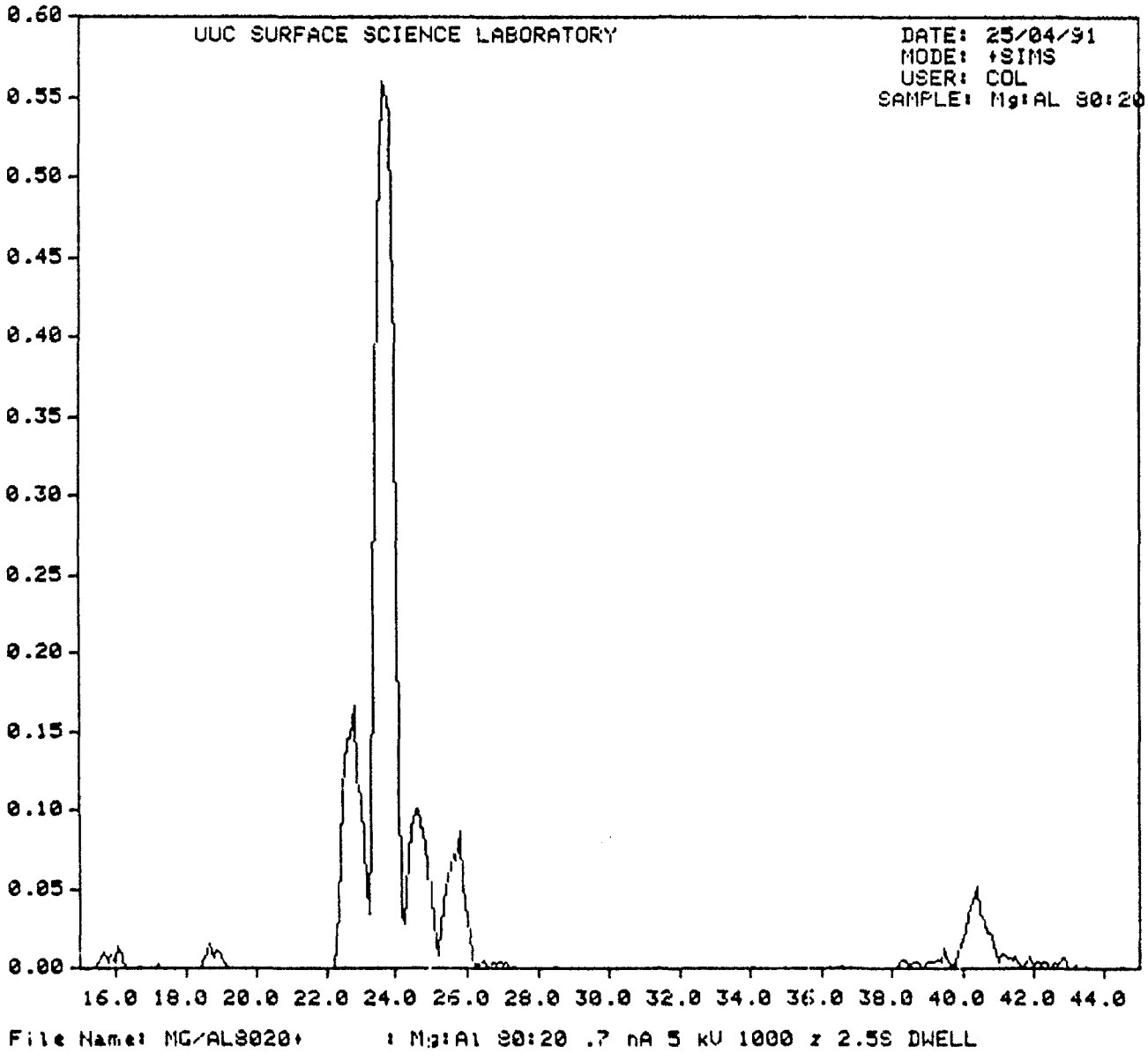
UUC SURFACE SCIENCE LABORATORY
DATE: 25/04/91
MODE: +SIMS
USER: COL
SAMPLE: Mg:AL 80:20
0.60
0.55
0.50
0.45
0.40
0.35
0.30
0.25
0.20
0.15
0.10
0.05
0.00
16.0 18.0 20.0 22.0 24.0 26.0 28.0 30.0 32.0 34.0 36.0 38.0 40.0 42.0 44.0
File Name: MG/AL8020+
: Mg:Al 80:20 .7 nA 5 kV 1000 x 2.5S DWELL

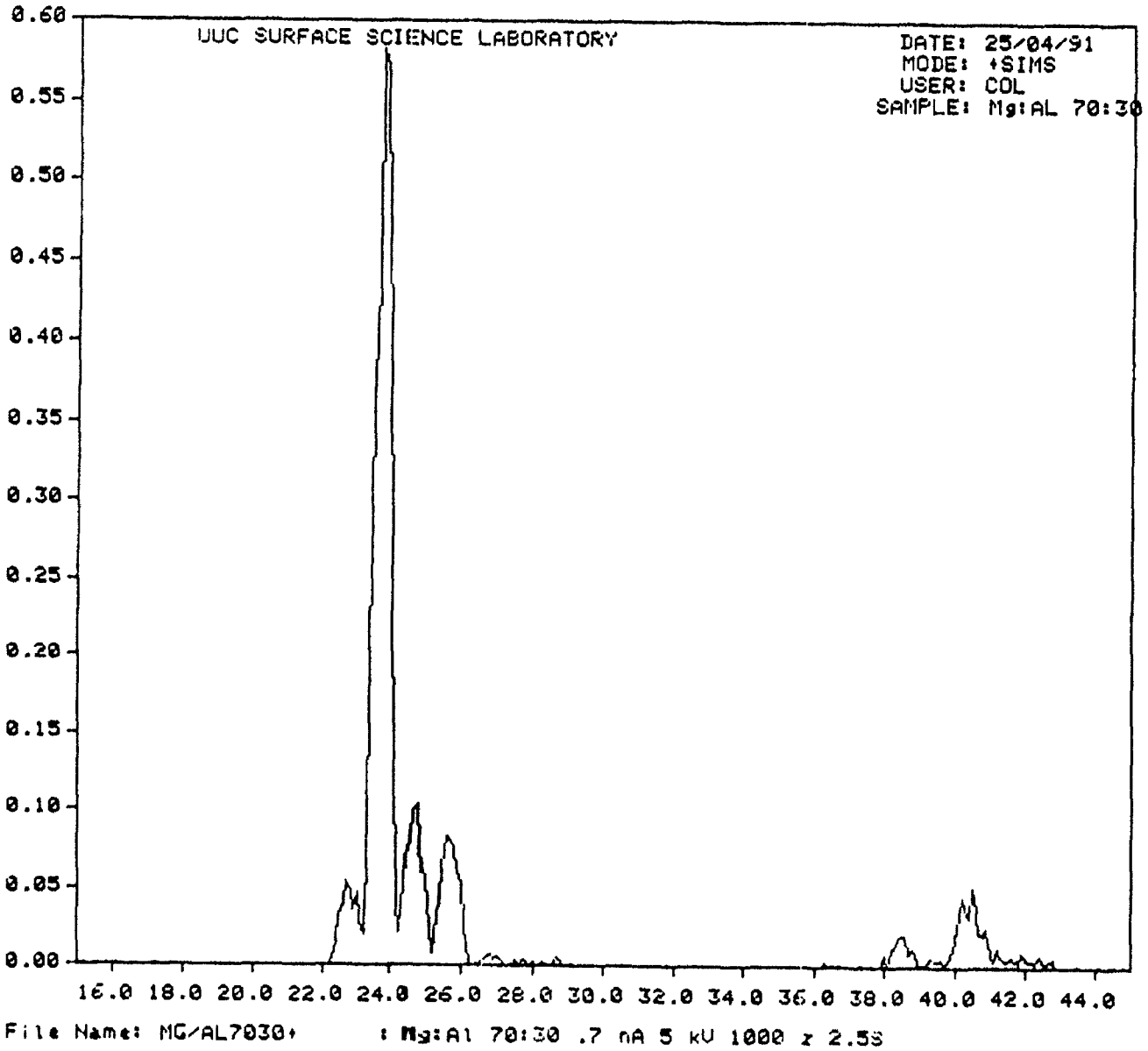
UUC SURFACE SCIENCE LABORATORY
DATE: 25/04/91
MODE: +SIMS
USER: COL
SAMPLE: Mg:AL 70:30
0.60
0.55
0.50
0.45
0.40
0.35
0.30
0.25
0.20
0.15
0.10
0.05
0.00
16.0 18.0 20.0 22.0 24.0 26.0 28.0 30.0 32.0 34.0 36.0 38.0 40.0 42.0 44.0
File Name: MG/AL7030+
: Mg:Al 70:30 .7 nA 5 kV 1000 x 2.5s

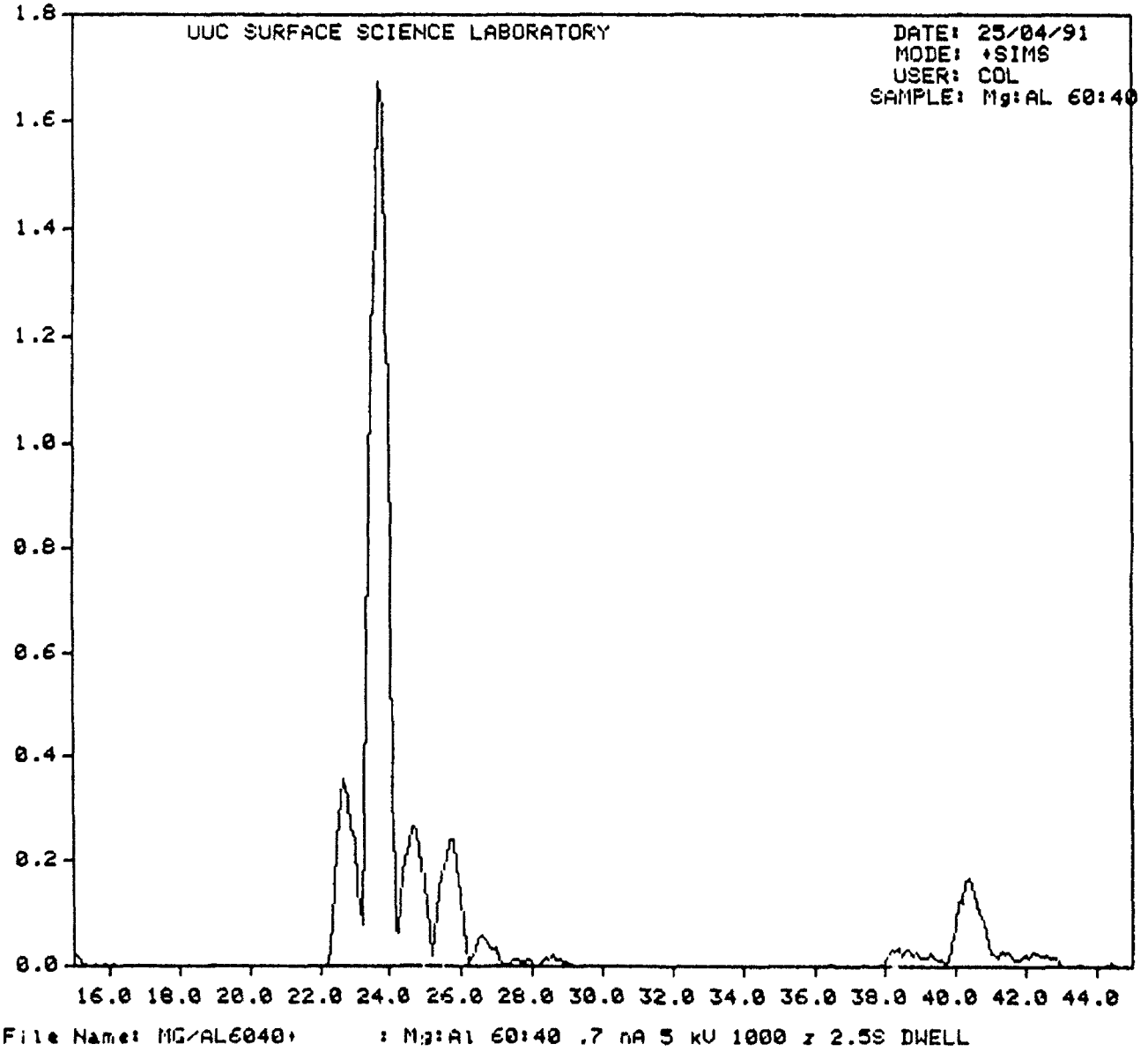
UUC SURFACE SCIENCE LABORATORY
DATE: 25/04/91
MODE: +SIMS
USER: COL
SAMPLE: Mg:AL 60:40
1.8
1.6
1.4
1.2
1.0
0.8
0.6
0.4
0.2
0.0
16.0 18.0 20.0 22.0 24.0 26.0 28.0 30.0 32.0 34.0 36.0 38.0 40.0 42.0 44.0
File Name: MG/AL6040+ : Mg:Al 60:40 .7 nA 5 kV 1000 x 2.5S DWELL

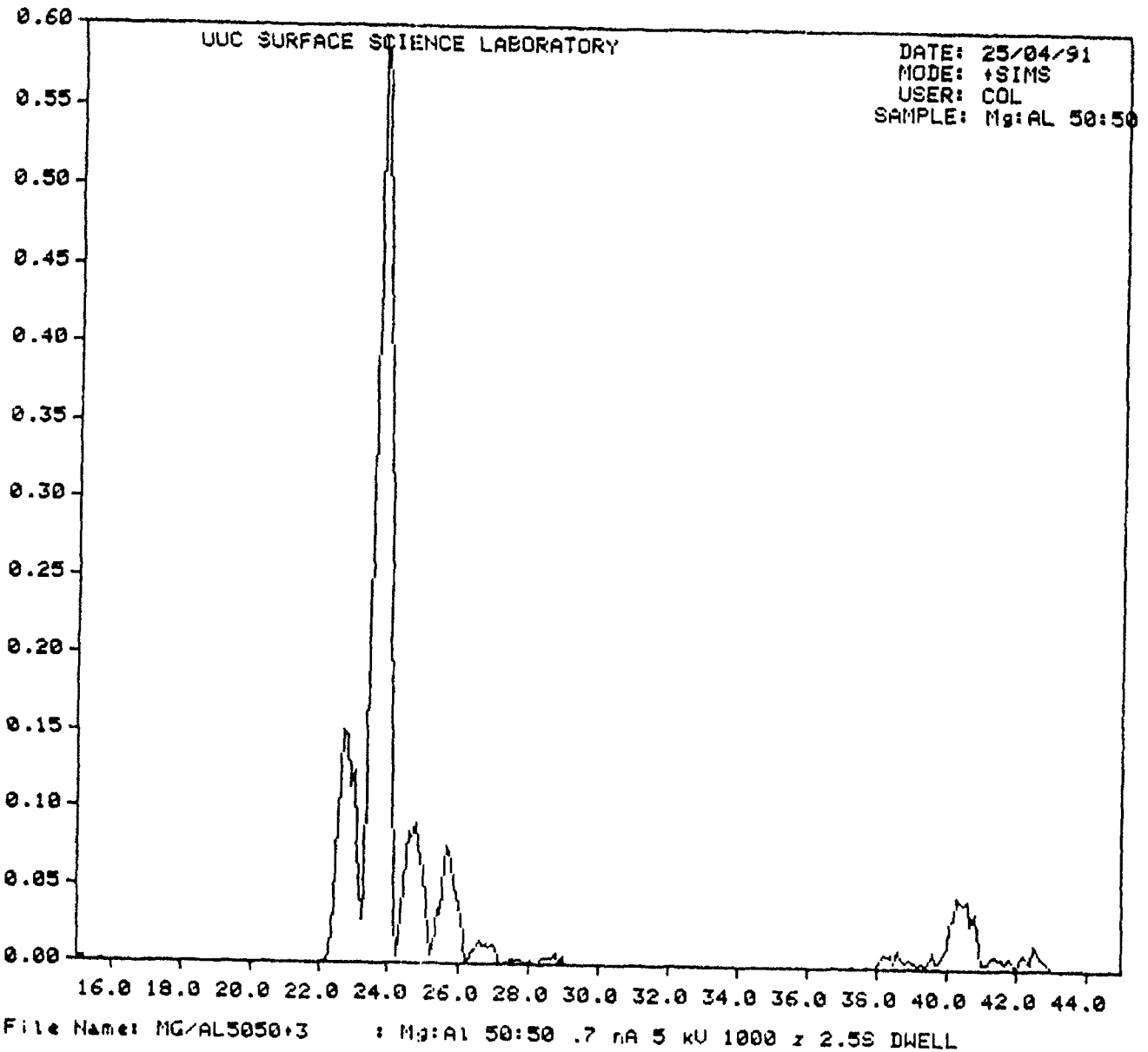
UUC SURFACE SCIENCE LABORATORY
DATE: 25/04/91
MODE: +SIMS
USER: COL
SAMPLE: Mg:AL 50:50
0.60
0.55
0.50
0.45
0.40
0.35
0.30
0.25
0.20
0.15
0.10
0.05
0.00
16.0 18.0 20.0 22.0 24.0 26.0 28.0 30.0 32.0 34.0 36.0 38.0 40.0 42.0 44.0
File Name: MG/AL5050+3 : Mg:Al 50:50 .7 nA 5 kV 1000 x 2.5S DWELL

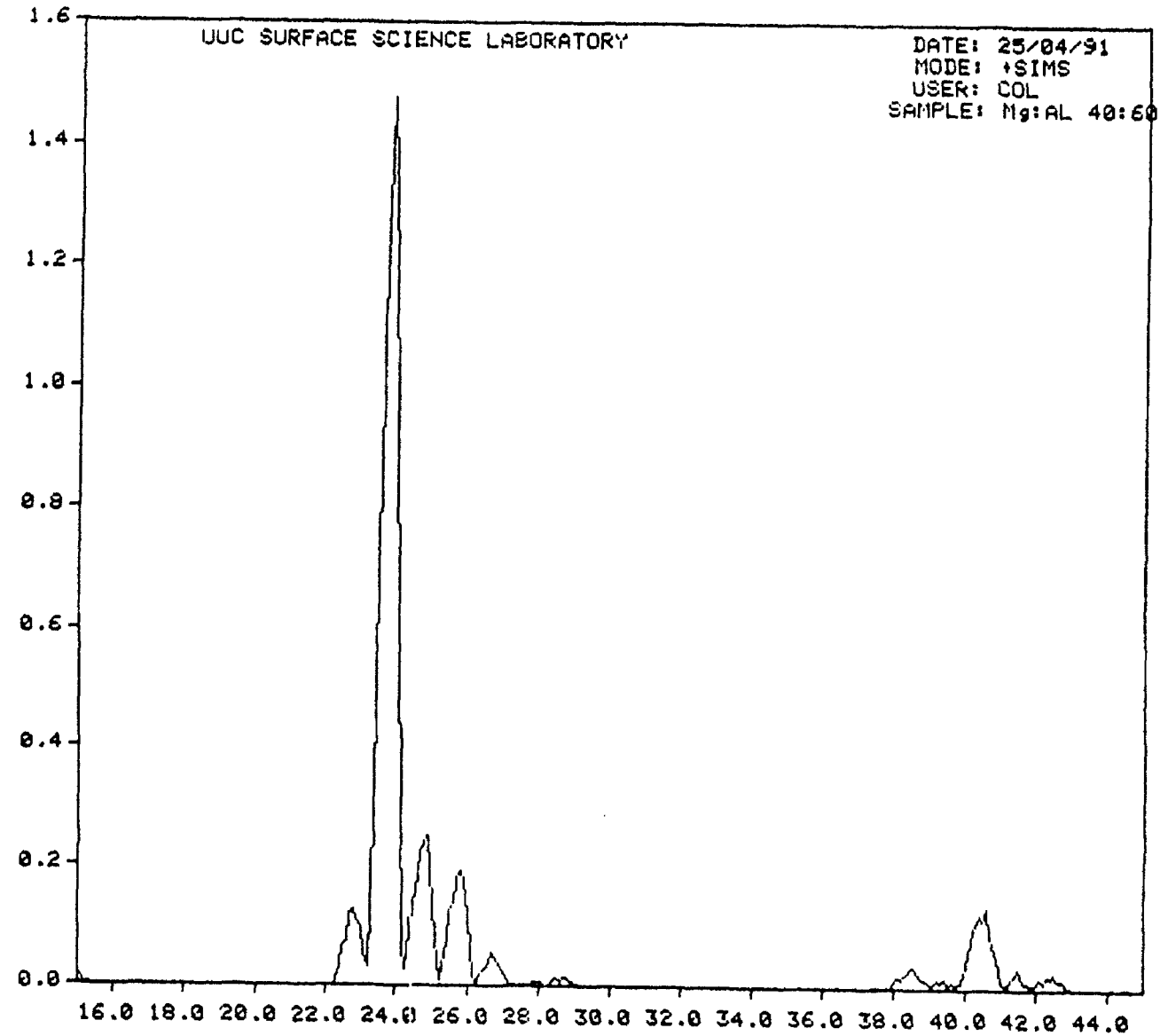
UUC SURFACE SCIENCE LABORATORY
DATE: 25/04/91
MODE: +SIMS
USER: COL
SAMPLE: Mg:AL 40:60
1.6
1.4
1.2
1.0
0.8
0.6
0.4
0.2
0.0
16.0 18.0 20.0 22.0 24.0 26.0 28.0 30.0 32.0 34.0 36.0 38.0 40.0 42.0 44.0
File Name: MG/AL4060+ : Mg:Al 40:60 .7 nA 5 kV 1000 x 2.5S DWELL

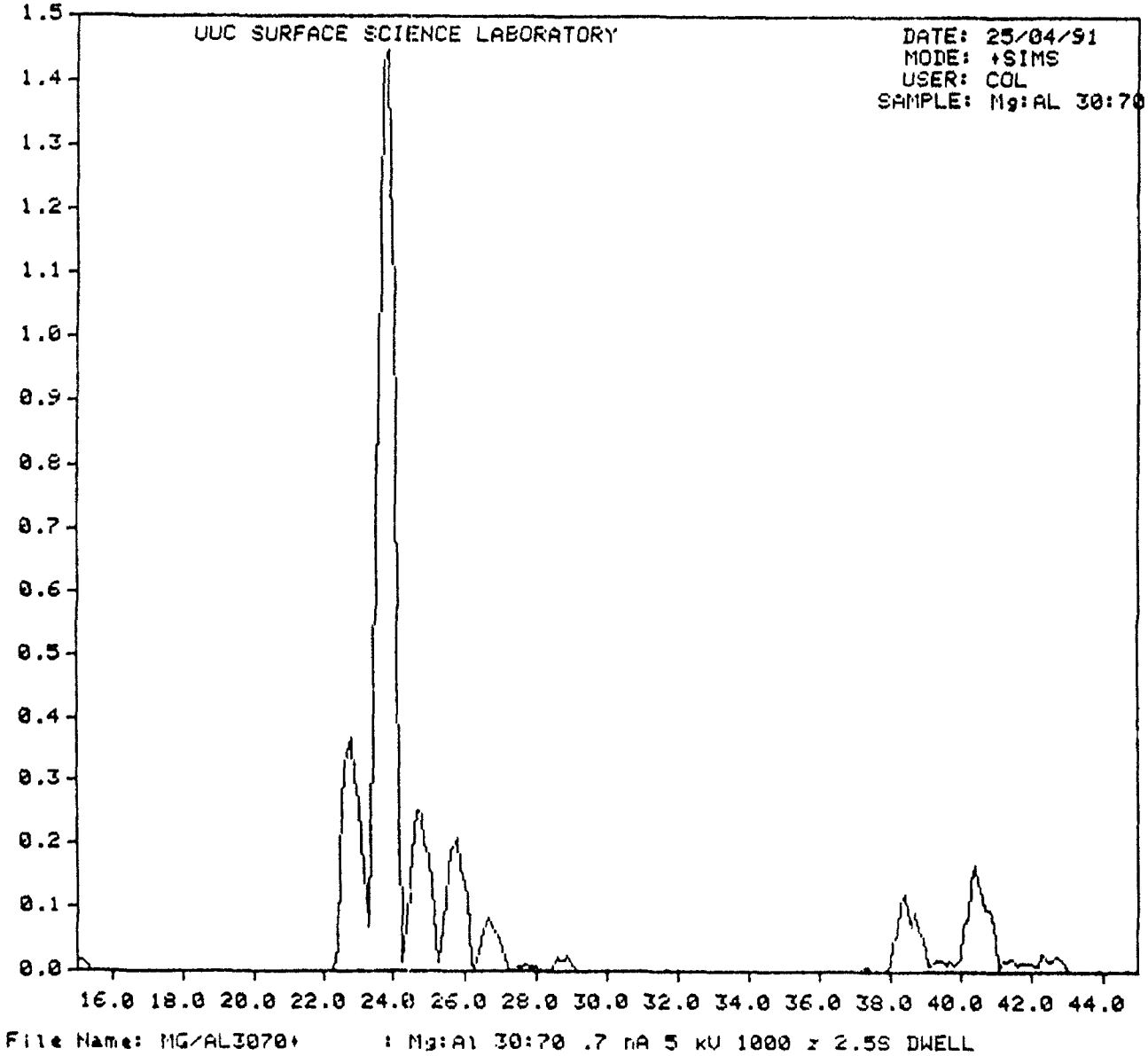
UUC SURFACE SCIENCE LABORATORY
DATE: 25/04/91
MODE: +SIMS
USER: COL
SAMPLE: Mg:AL 30:70
1.5
1.4
1.3
1.2
1.1
1.0
0.9
0.8
0.7
0.6
0.5
0.4
0.3
0.2
0.1
0.0
16.0 18.0 20.0 22.0 24.0 26.0 28.0 30.0 32.0 34.0 36.0 38.0 40.0 42.0 44.0
File Name: MG/AL3070+ : Mg:Al 30:70 .7 nA 5 kV 1000 x 2.5S DWELL

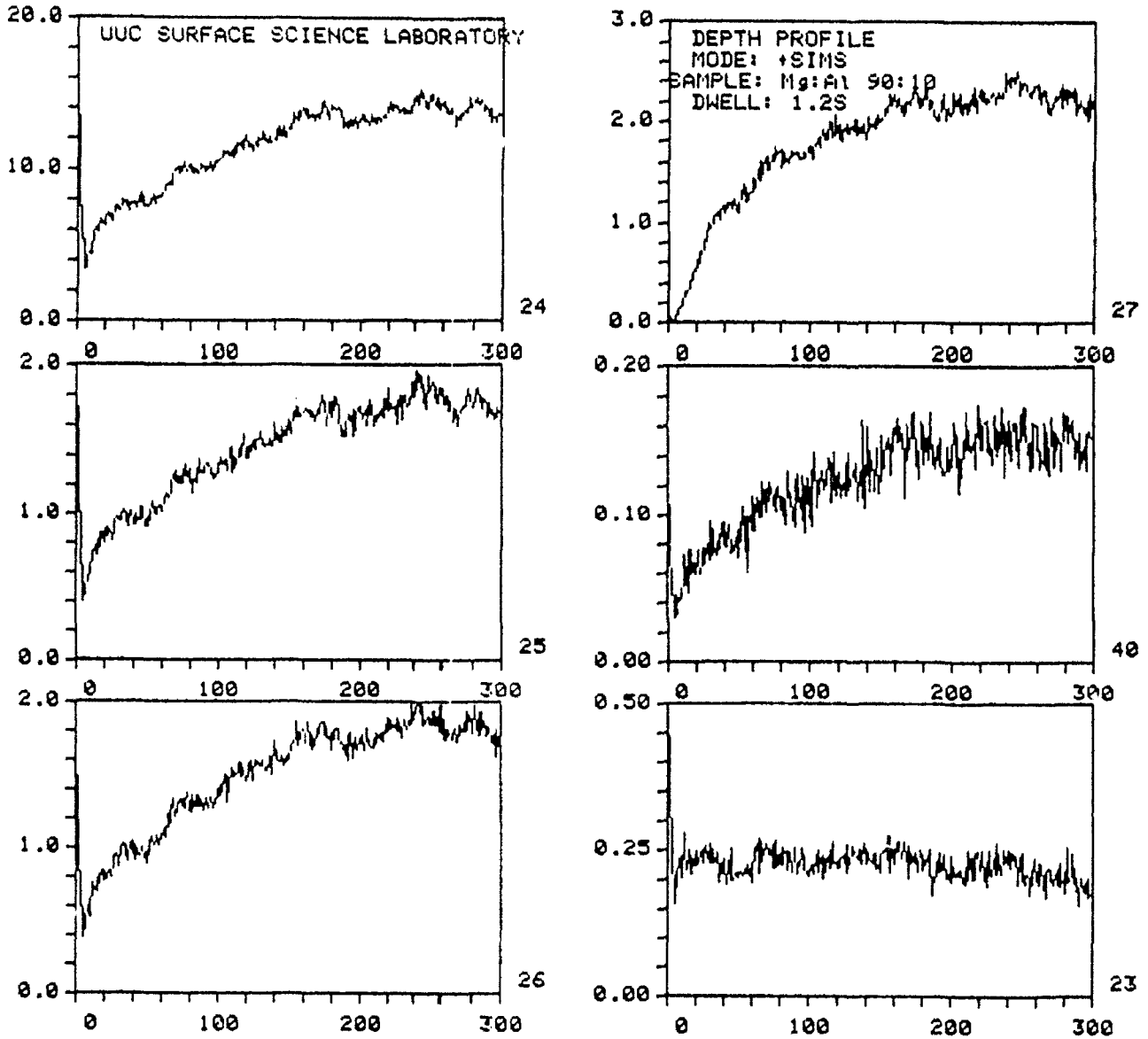

File Name: MG/AL9010PRO+1 Title: Depth profile 70nA 5kV 200x 100% gate

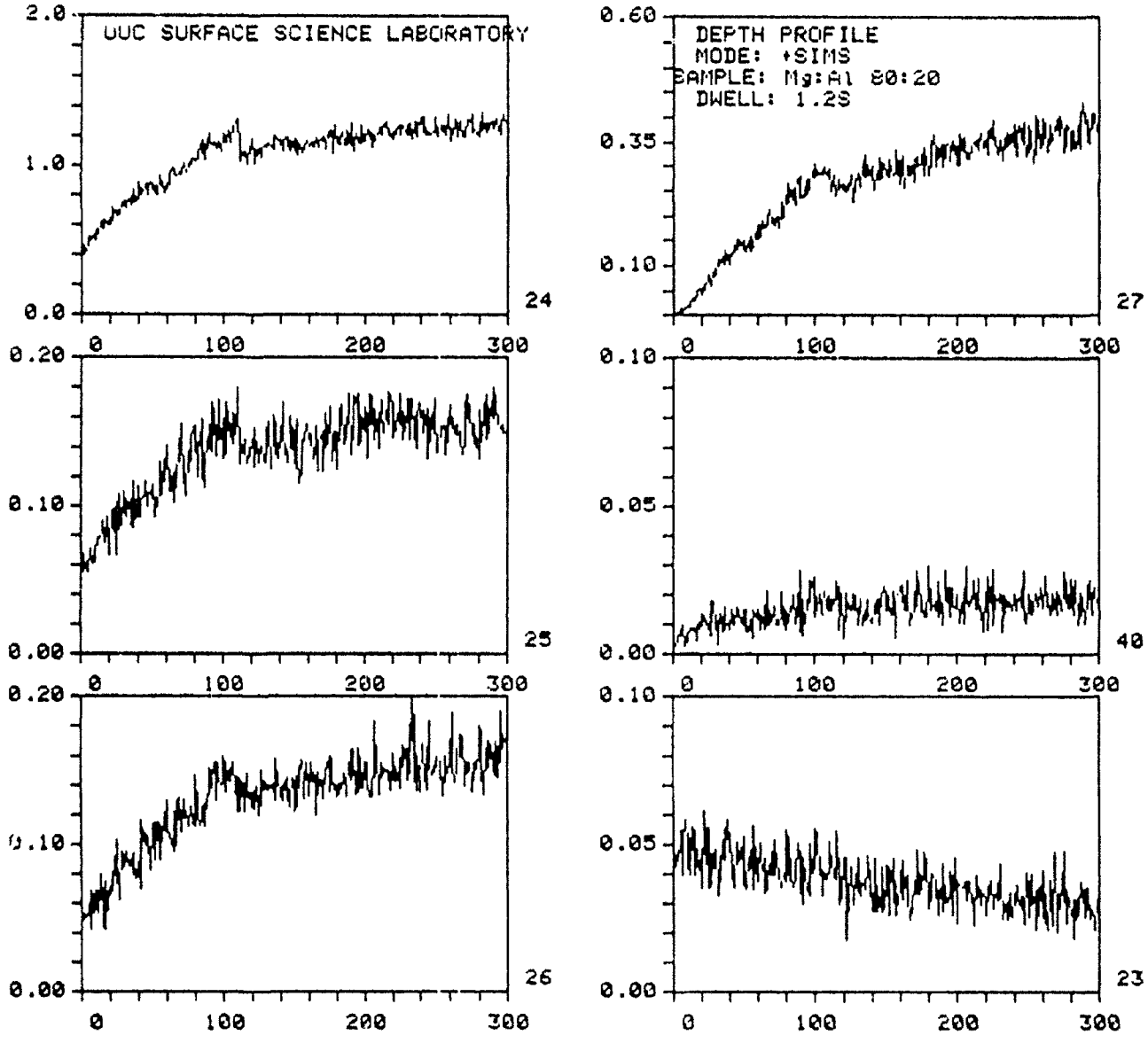
UUC SURFACE SCIENCE LABORATORY
DEPTH PROFILE
MODE: +SIMS
SAMPLE: Mg:Al 80:20
DWELL: 1.2S
2.0
1.0
0.0
0.60
0.35
0.10
0.20
0.10
0.00
0.05
0.10
0.05
0
100
200
300
24
27
25
40
26
23
File Name: MG/AL9020PRO+ Title: Depth profile 70nA 5kV 200x 100% gate

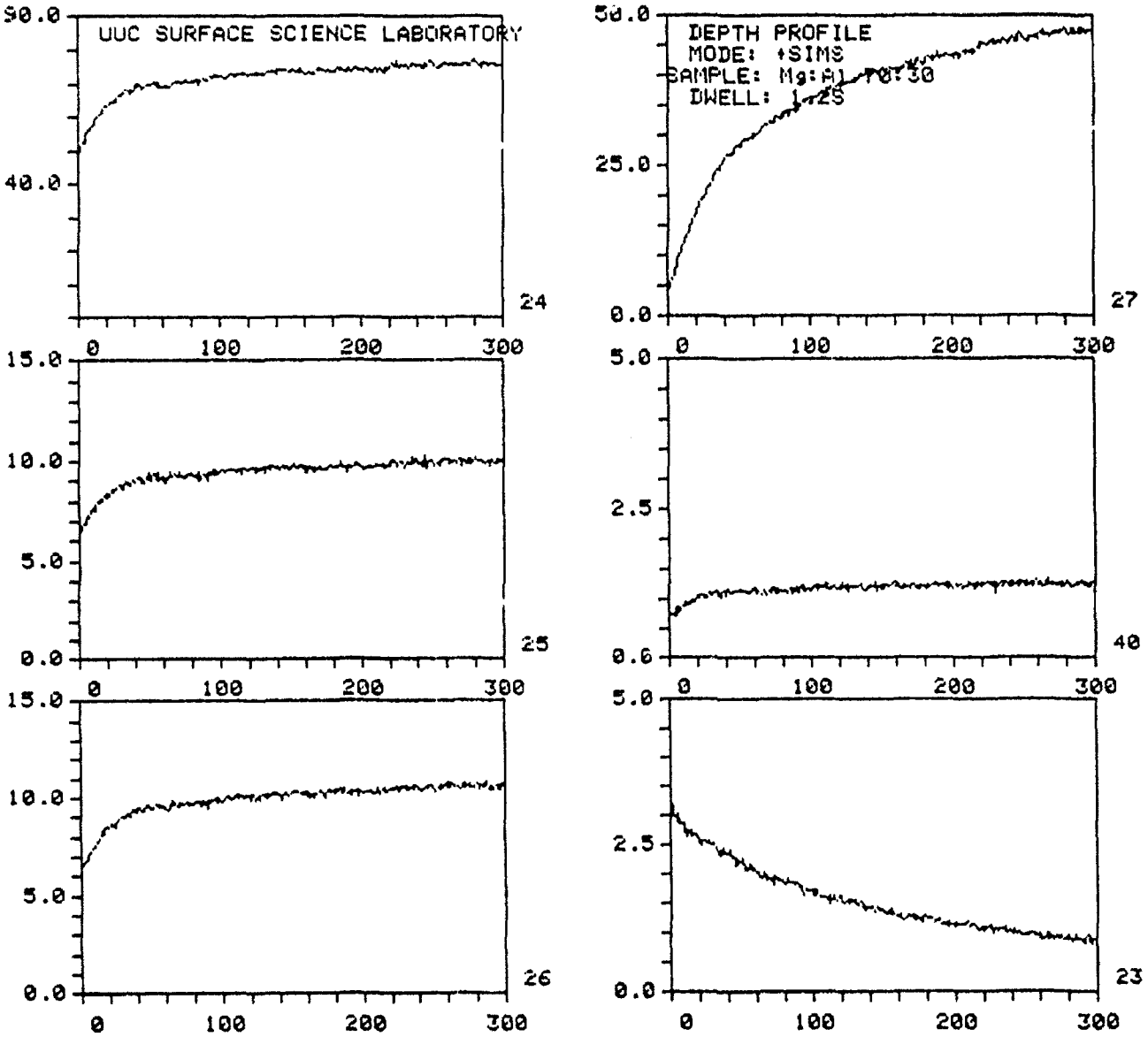

File Name: MG/AL7030PRO+1 Title: Depth profile 70nA 5kV 200x 100% gate

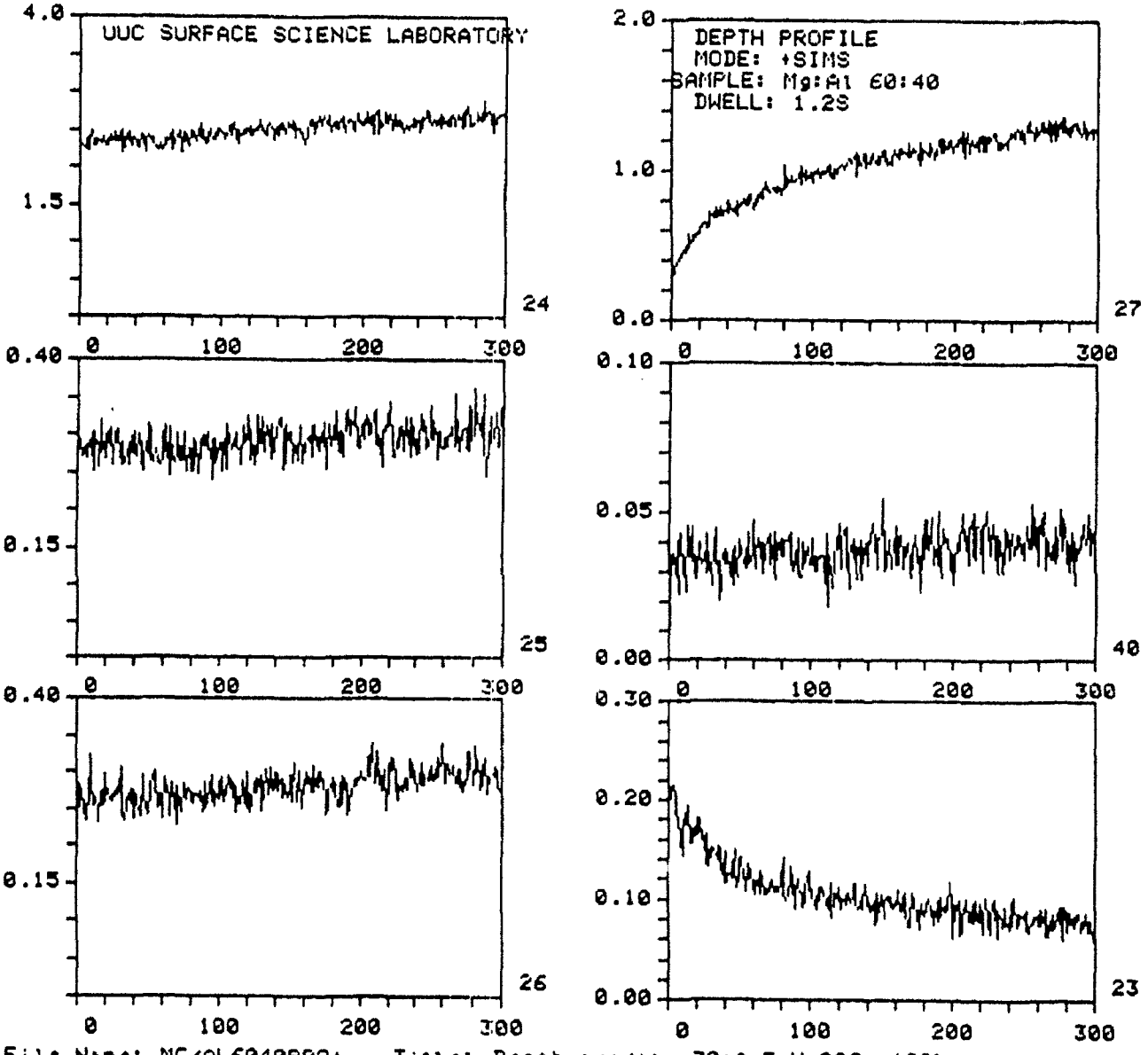
UUC SURFACE SCIENCE LABORATORY
DEPTH PROFILE
MODE: +SIMS
SAMPLE: Mg:Al 60:40
DWELL: 1.2S
4.0
1.5
24
2.0
1.0
0.0
27
0.40
0.15
25
0.10
0.05
0.00
40
0.40
0.15
26
0.30
0.20
0.10
0.00
23
0
100
200
300
File Name: MG/AL6040PRO+ Title: Depth profile 70nA 5kV 200x 100% gate

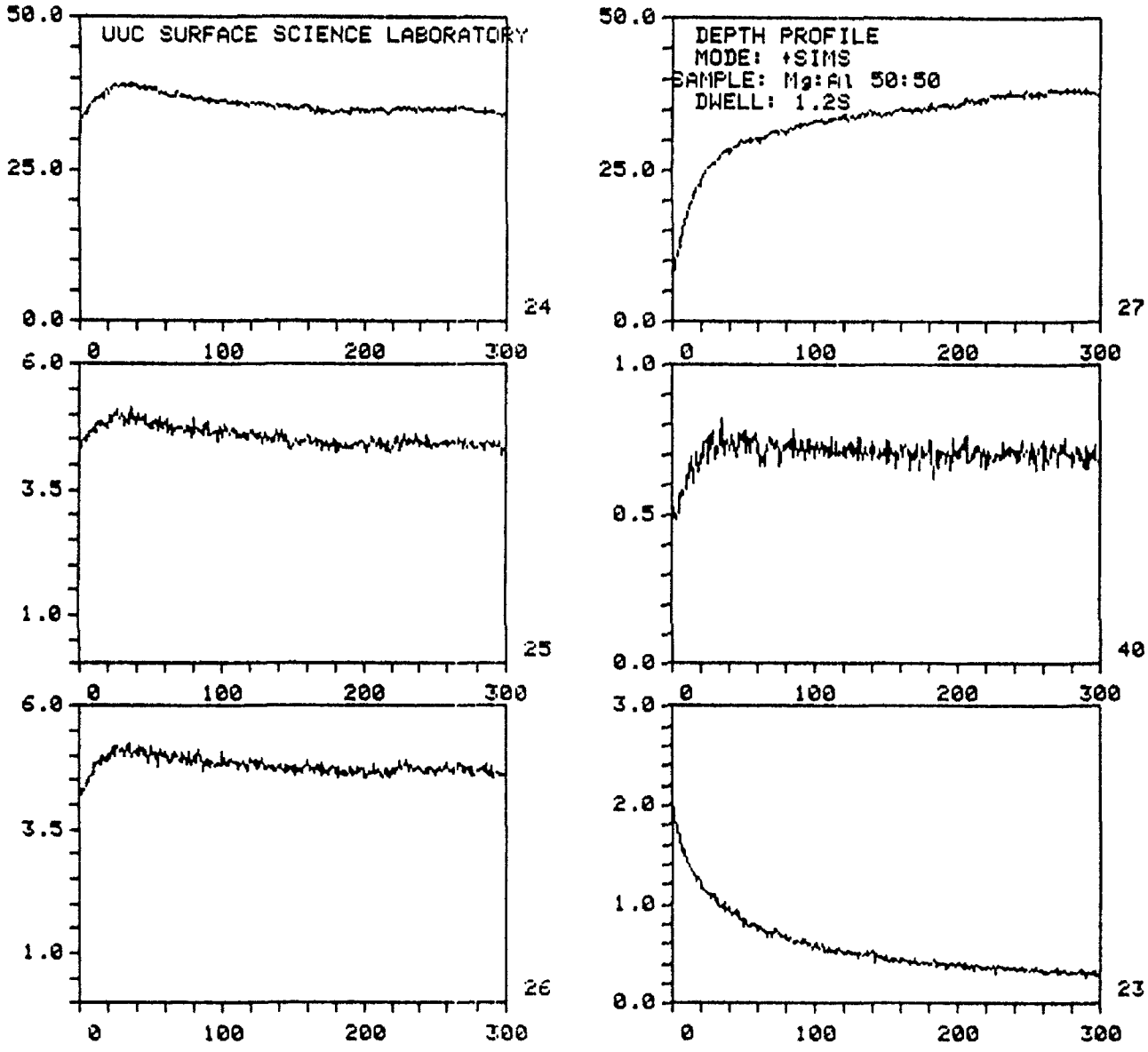

File Name: MG/AL5050PRO+1 Title: Depth profile 70nA 5kV 200x 100% gate

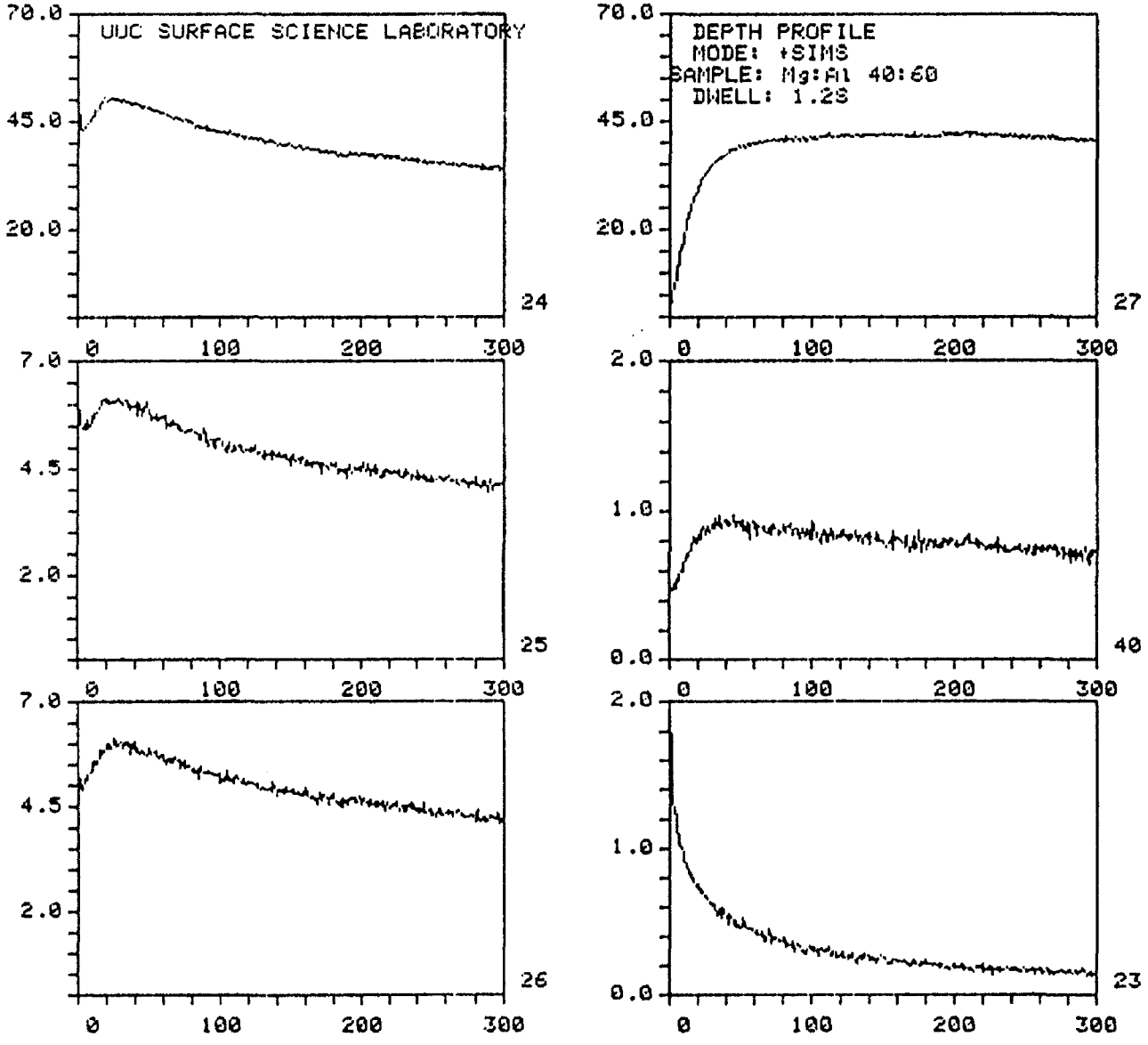

File Name: MG/AL4060PRO+ Title: Depth profile 70nA 5kV 200z 100% gate

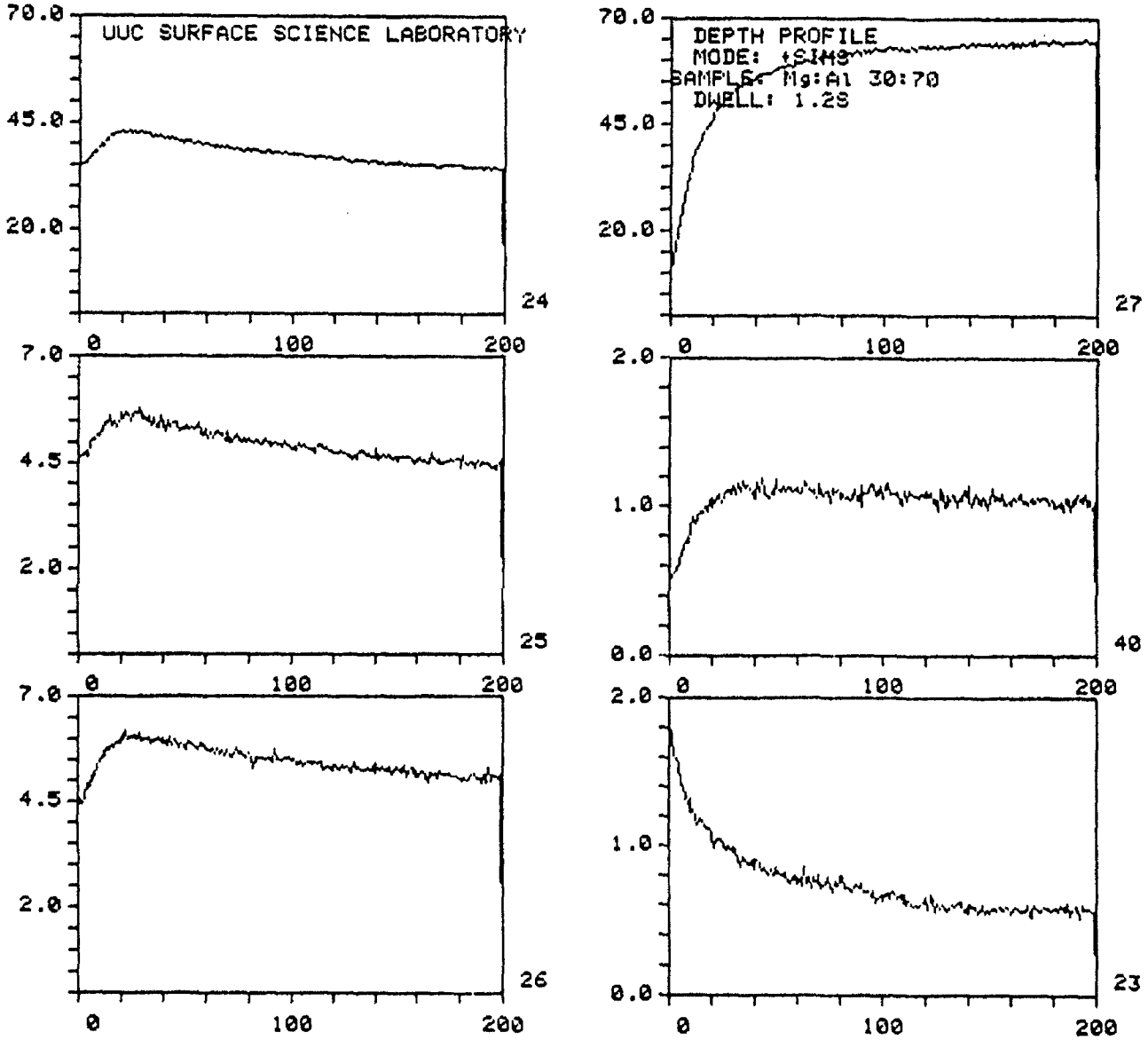

File Name: MG/AL3070PRO+3 Title: Depth profile 70nA 5kV 200x 100% gate

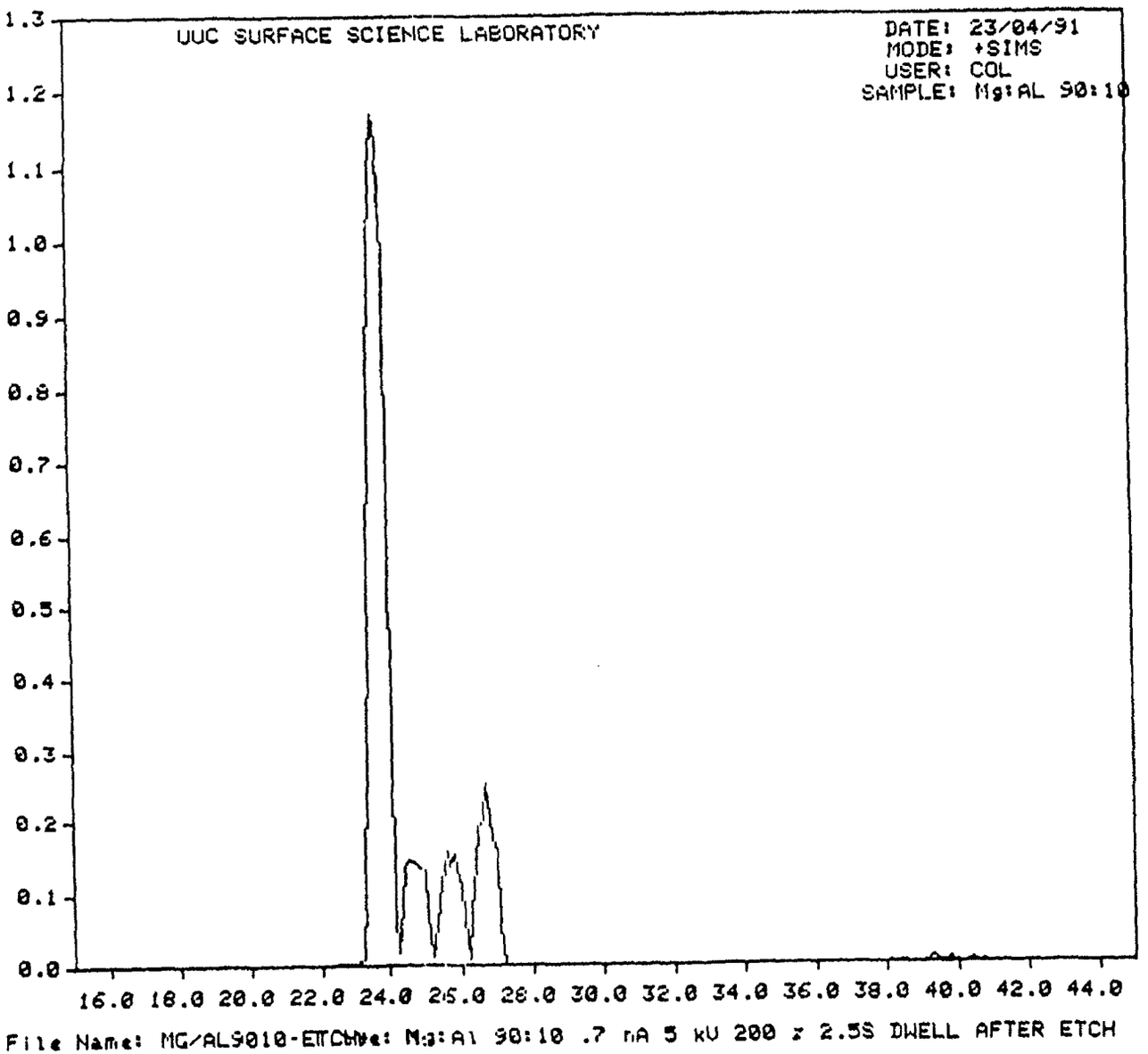
UUC SURFACE SCIENCE LABORATORY
DATE: 23/04/91
MODE: +SIMS
USER: COL
SAMPLE: Mg:AL 90:10
1.3
1.2
1.1
1.0
0.9
0.8
0.7
0.6
0.5
0.4
0.3
0.2
0.1
0.0
16.0 18.0 20.0 22.0 24.0 26.0 28.0 30.0 32.0 34.0 36.0 38.0 40.0 42.0 44.0
File Name: MG/AL9010-ETCH Mg:Al 90:10 .7 nA 5 kV 200 x 2.5S DWELL AFTER ETCH

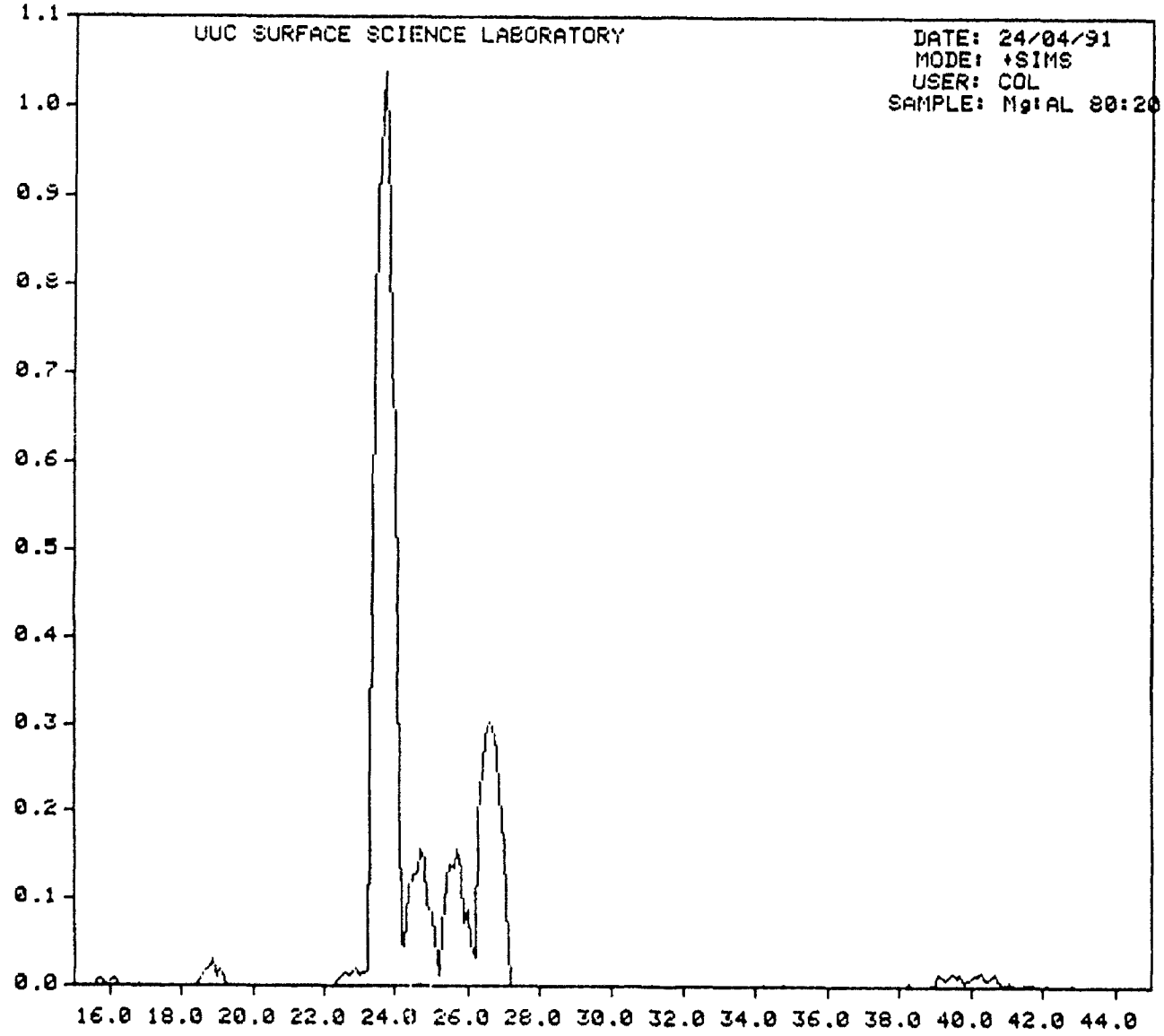
UUC SURFACE SCIENCE LABORATORY
DATE: 24/04/91
MODE: +SIMS
USER: COL
SAMPLE: Mg:AL 80:20
1.1
1.0
0.9
0.8
0.7
0.6
0.5
0.4
0.3
0.2
0.1
0.0
16.0 18.0 20.0 22.0 24.0 26.0 28.0 30.0 32.0 34.0 36.0 38.0 40.0 42.0 44.0
File Name: MG/ALS020-ETCH+ : Mg:Al 80:20 .7 nA 5 kV 200 x 2.5S DWELL AFTER ETCH

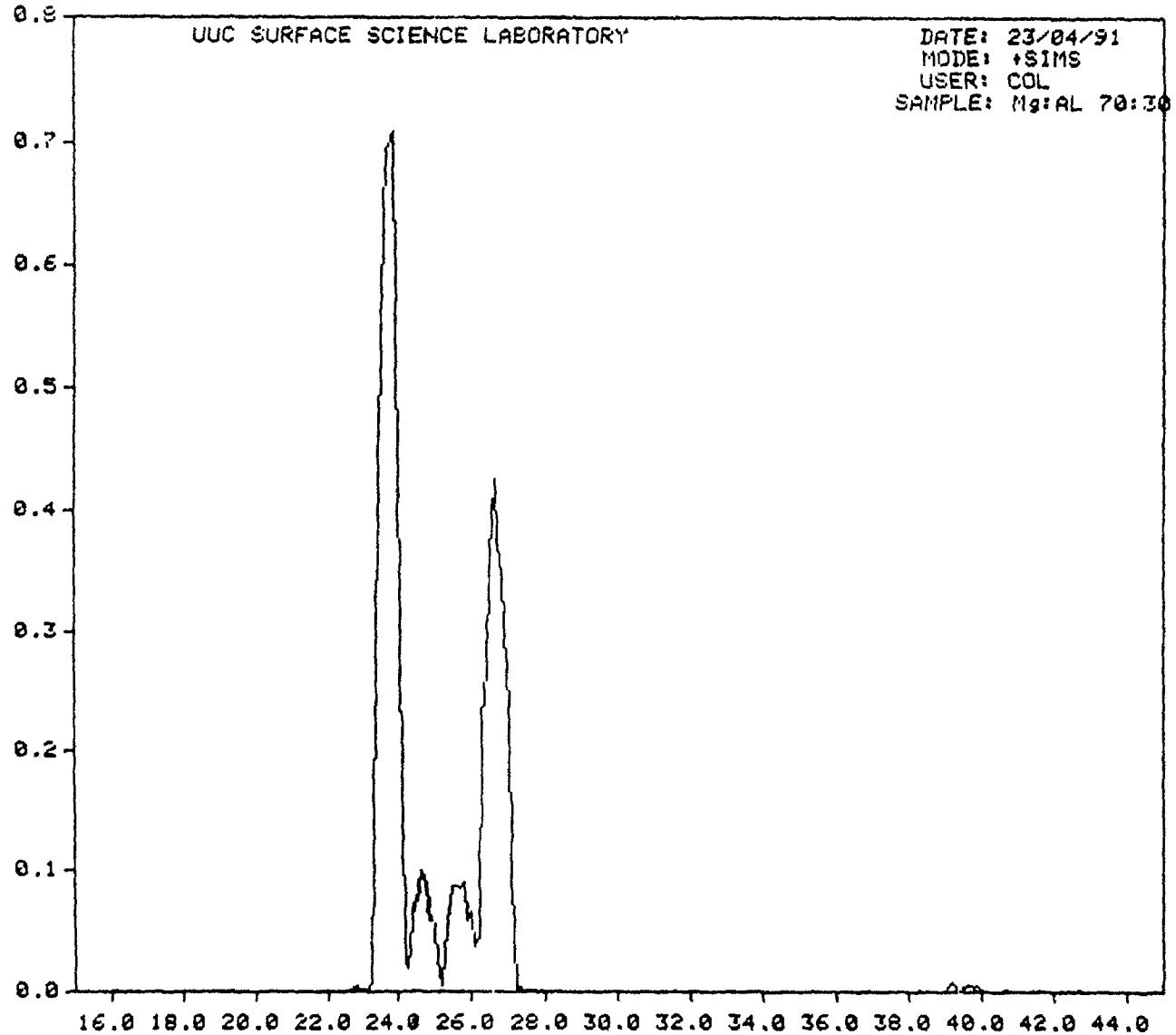

File Name: MG/AL7030-ETCH Mg:Al 70:30 .7 nA 5 kV 200 x 2.5S DWELL AFTER ETCH

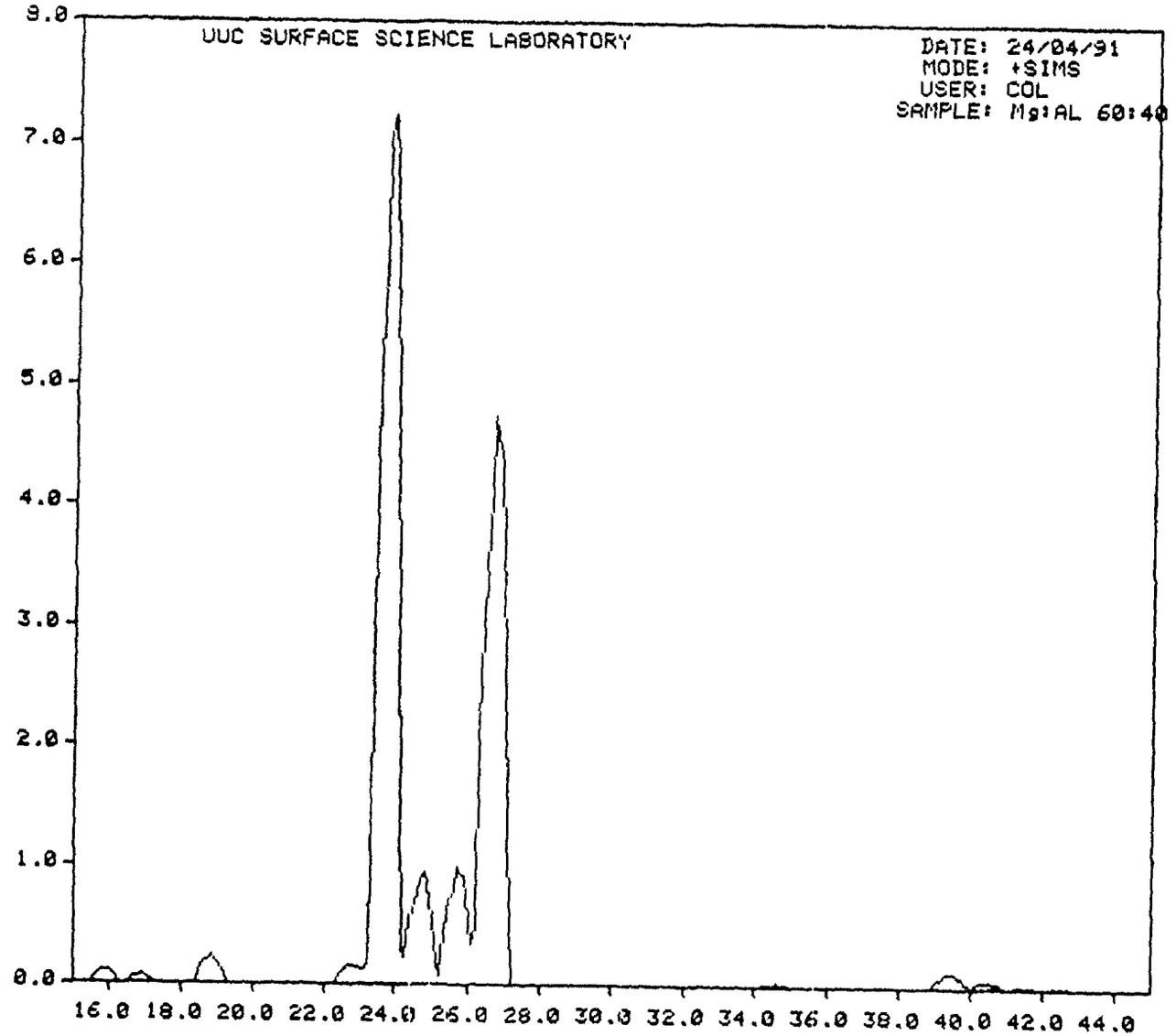
UUC SURFACE SCIENCE LABORATORY
DATE: 24/04/91
MODE: +SIMS
USER: COL
SAMPLE: Mg:AL 60:40
9.0
7.0
6.0
5.0
4.0
3.0
2.0
1.0
0.0
16.0 18.0 20.0 22.0 24.0 26.0 28.0 30.0 32.0 34.0 36.0 38.0 40.0 42.0 44.0
File Name: MG/AL6040-ETCH+ : Mg:Al 60:40 .7 nA 5 kV 200 x 2.5S DWELL AFTER ETCH

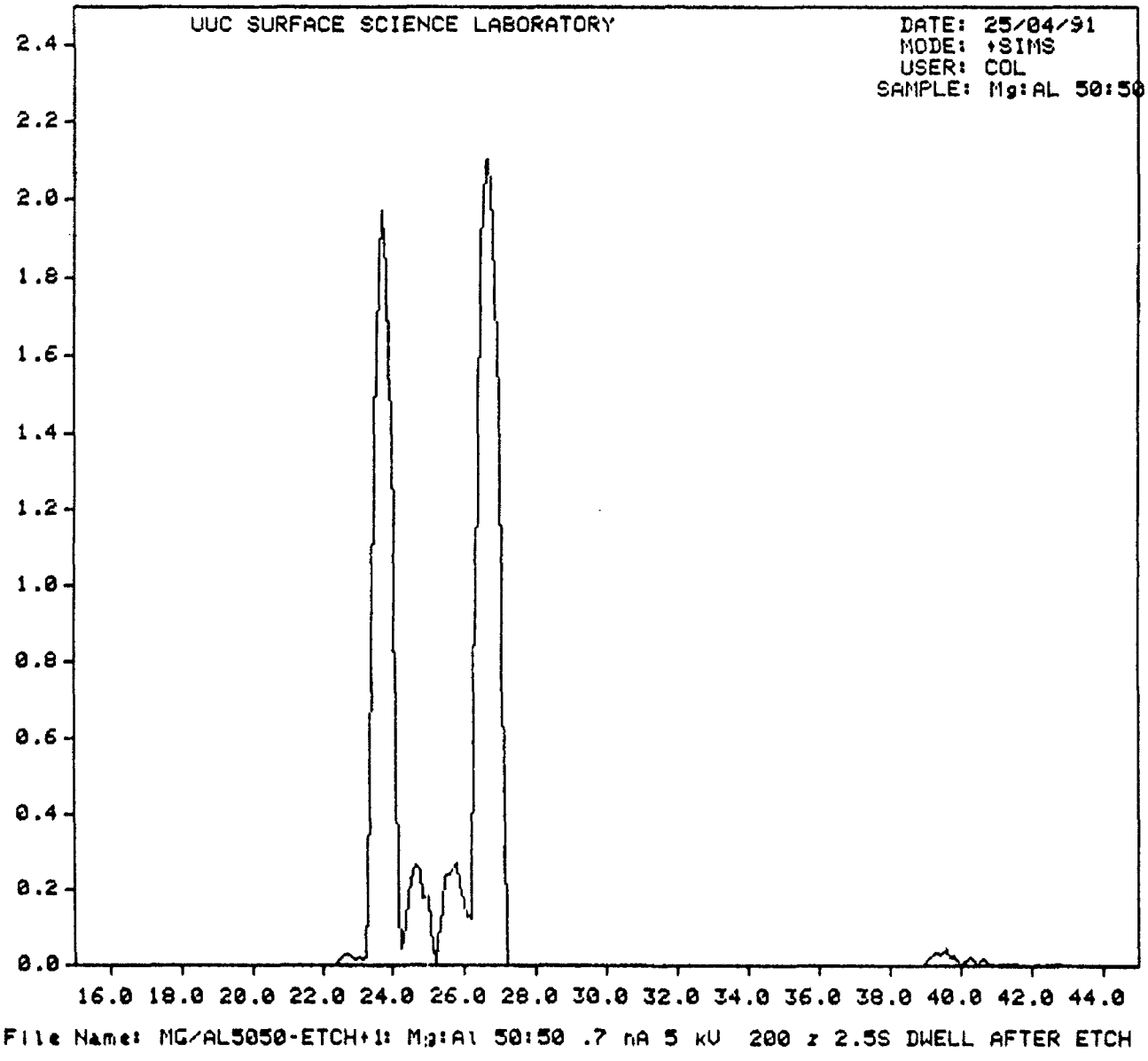
UUC SURFACE SCIENCE LABORATORY
DATE: 25/04/91
MODE: +SIMS
USER: COL
SAMPLE: Mg:AL 50:50
2.4
2.2
2.0
1.8
1.6
1.4
1.2
1.0
0.8
0.6
0.4
0.2
0.0
16.0 18.0 20.0 22.0 24.0 26.0 28.0 30.0 32.0 34.0 36.0 38.0 40.0 42.0 44.0
File Name: MG/AL5050-ETCH+1: Mg:Al 50:50 .7 nA 5 kV 200 x 2.5S DWELL AFTER ETCH

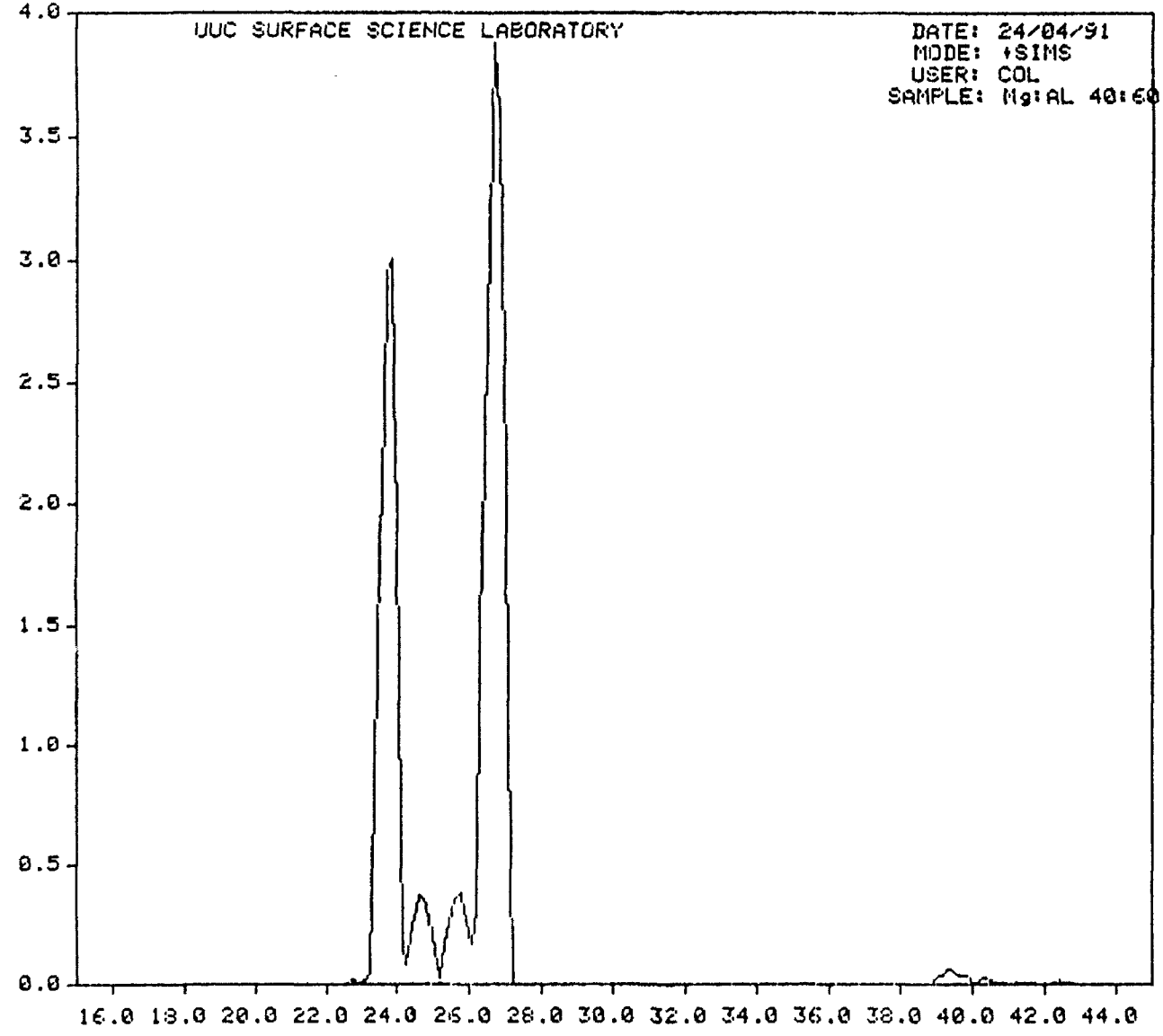
UUC SURFACE SCIENCE LABORATORY
DATE: 24/04/91
MODE: +SIMS
USER: COL
SAMPLE: Mg:AL 40:60
4.0
3.5
3.0
2.5
2.0
1.5
1.0
0.5
0.0
16.0 18.0 20.0 22.0 24.0 26.0 28.0 30.0 32.0 34.0 36.0 38.0 40.0 42.0 44.0
File Name: MG/AL4060-ETCH+ : Mg:Al 40:60 .7 nA 5 kV 200 x 2.5S DWELL AFTER ETCH

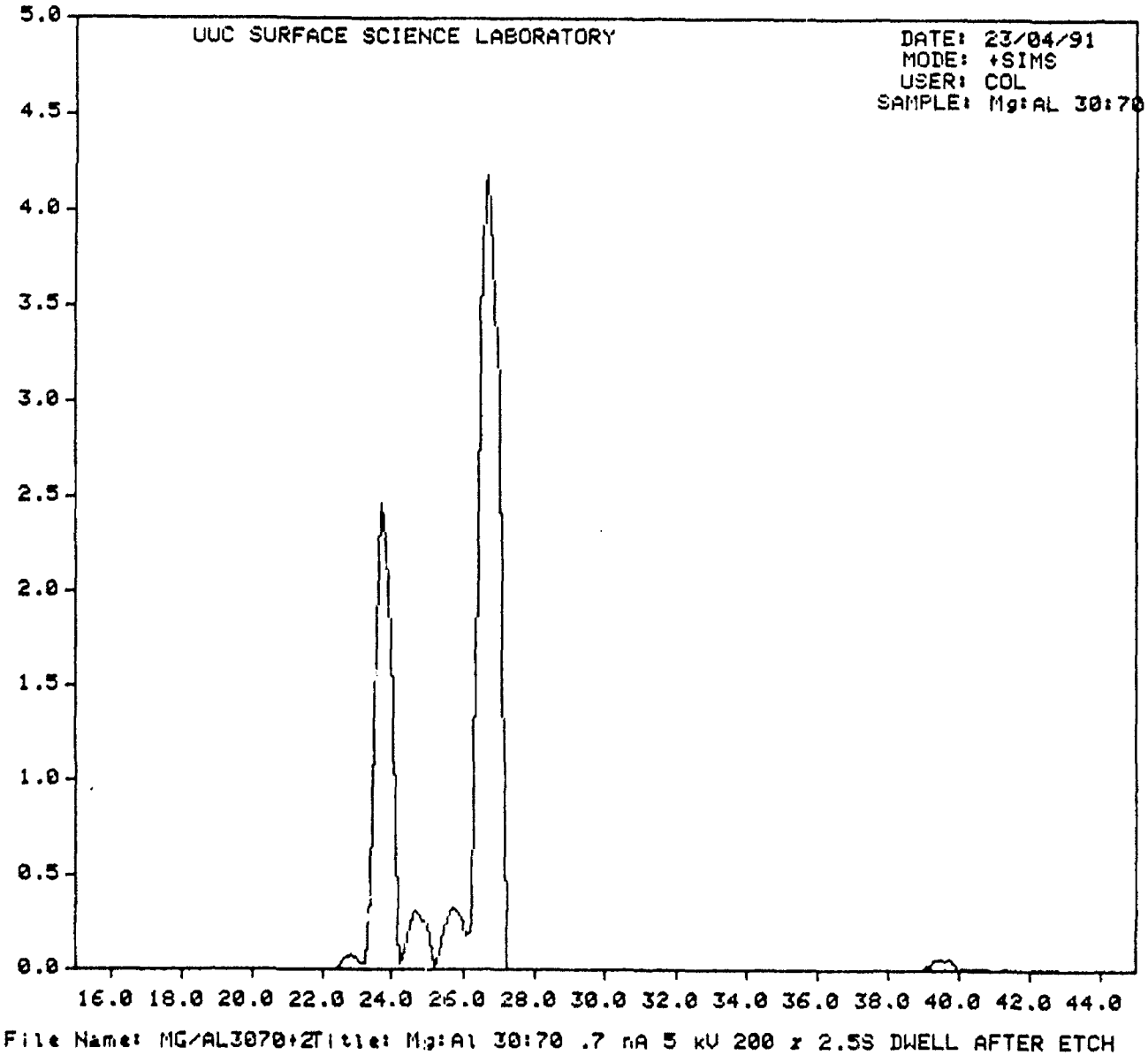
UUC SURFACE SCIENCE LABORATORY
DATE: 23/04/91
MODE: +SIMS
USER: COL
SAMPLE: Mg:AL 30:70
5.0
4.5
4.0
3.5
3.0
2.5
2.0
1.5
1.0
0.5
0.0
16.0 18.0 20.0 22.0 24.0 26.0 28.0 30.0 32.0 34.0 36.0 38.0 40.0 42.0 44.0
File Name: MG/AL3070+2Title: Mg:Al 30:70 .7 nA 5 kV 200 x 2.5S DWELL AFTER ETCH

Examination of the spectra of the 'real' surface show an intense magnesium signal indicative of a high presence of magnesium on the surfaces of the alloys. Smaller peaks are also observed for aluminium and magnesium oxide but these are much weaker in intensity in comparison to the magnesium. These signals indicate a presence of aluminium and magnesium oxide on the surface but these are not the most prelevant species on the surface of the alloys.

Depth profiles initially show an increase in the aluminium signal suggesting an increasing aluminium presence within the bulk of the alloy particle. The aluminium signal is very intense indicating high amounts of aluminium in the alloy. The magnesium signals are constant and high throughout the etching suggesting an even distribution of magnesium throughout the alloy. The sodium signal decreases with further etching suggesting less sodium impurity within the 'core' of the alloy. The low signal intensity recorded for sodium indicates the sodium content in the alloy to be very low.

The final static SIMS spectra show quite a change in comparison to that of the 'real' surface. imediately intense aluminium and magnesium signals are observed. These intense signals indicate that both aluminium and magnesium are the two prelevant elements on the sub-surface. The other signals observed are indicative of sodium and magnesium oxide but both signals are small indicating very little sodium or magnesium oxide on the sub-surface.

3.3 Rheological analysis of magnesium/aluminium alloys

Rheological analysis of the alloys was performed on a Carri-med Controlled Stress Rheometer (CSR). Each alloy was

dispersed 40% w/w in CTBN 1300*15. The dispersed alloy was subjected to the conditions shown in figure 5. Rheological analysis of each alloy was repeated three times.

The results obtained from these experiments can be shown clearly in figure 6.

Figure 6 : Rheological analysis of alloys.

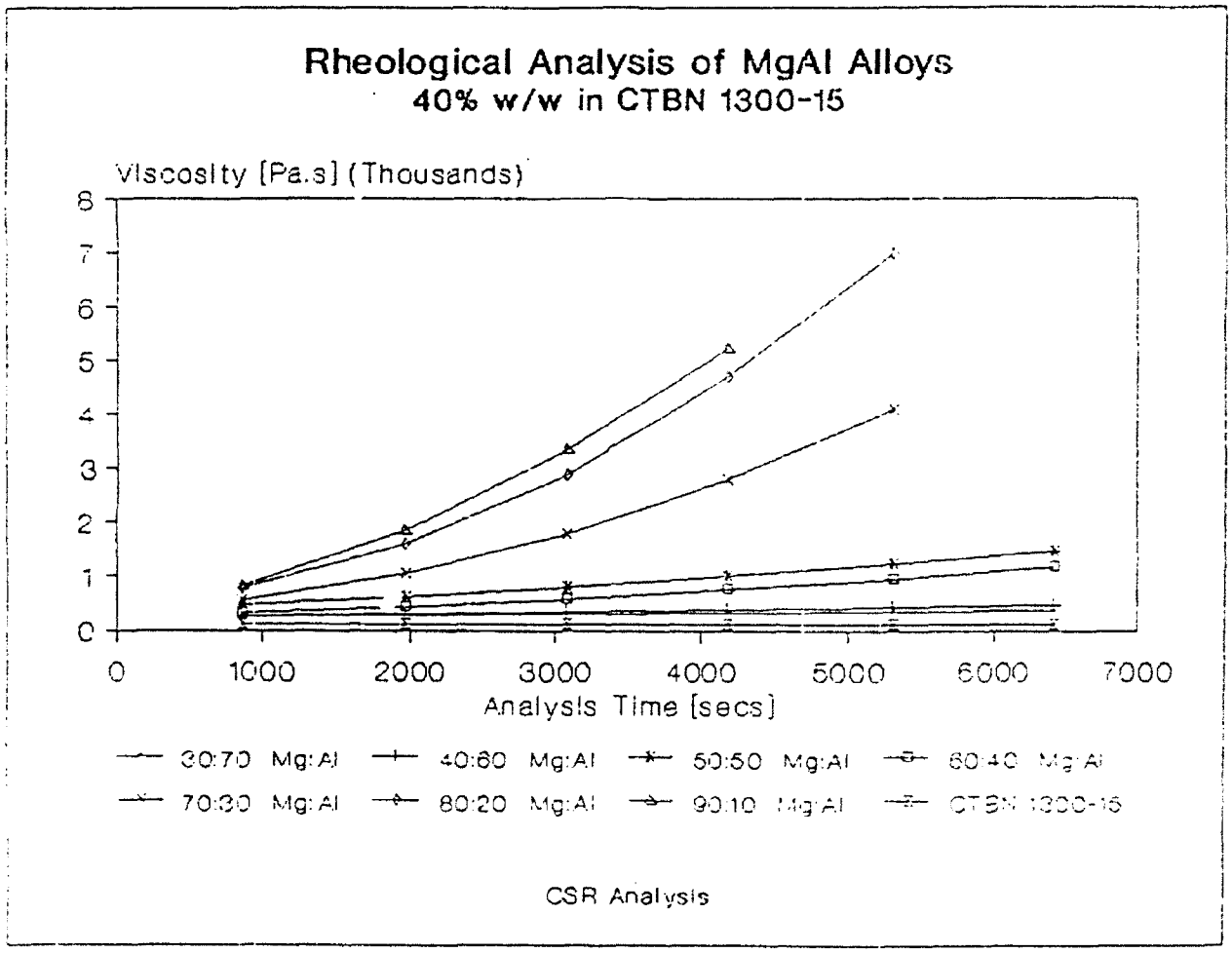

Figure 6 clearly shows that each alloy reacts with the polymer producing a viscosity increase with time. However, alloys with a high nominal value of aluminium have a slower change in rate of viscosity with time than those with higher nominal values of magnesium. These results suggest that the presence of the aluminium in the alloy has either, a much slower interaction with the acid end groups of the polymer than magnesium, interacts with the polymer in a complex way or does not react with the polymer. The curing reaction between magnesium and CTBN producing the large increase in viscosity is beginning to accelerate for alloys with a magnesium content greater than 70%. This suggests that alloys with a nominal value greater or equal to 70% have similar rheological properties to pure magnesium metal.

CHAPTER 4 : DISCUSSION

4.1 Static SIMS of alloy surfaces

Examination of the static SIMS spectra obtained for the alloys show a high signal intensity at mass number 24 (most abundant isotope of magnesium). Other smaller peaks are also observed at 23 (sodium impurity within the alloy), 25, 26 (less abundant isotopes of magnesium), 27 (aluminium) and 40, 41 (magnesium oxide). These signals indicate that the alloy surfaces are highly abundant in magnesium and less abundant in an magnesium oxide overlayer and aluminium.

However, signal intensities alone can not simply be used to quantify the amounts of specific elements on a surface. Under different analysis conditions, different elements will give different secondary ion sputter yields. The secondary ion sputter yield for a molecular or atomic particle is defined as the number of particles sputtered divided by the number of impinging primary ions. The secondary ion sputter yields of magnesium and aluminium are very similar under different experimental conditions. This can be more clearly illustrated in figures 7 and 8. Figure 7 illustrates the absolute secondary ion sputter yields of selected elements under high vacuum conditions and under oxygen saturation.

Figure 7: Absolute secondary ion sputter yields as a function of atomic number.

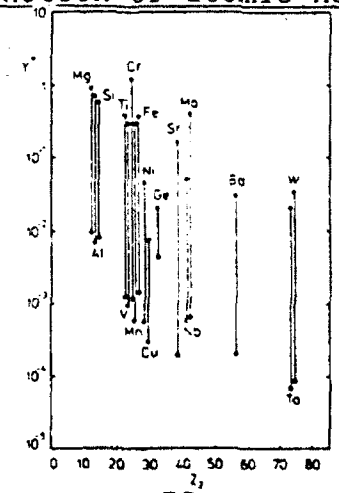

Figure 8 shows the relative positive ion sputter yields of selected elements under oxygen ion bombardment.

Figure 8: The relative positive ion sputter yields of selected elements using a 13.5keV O^- gun.

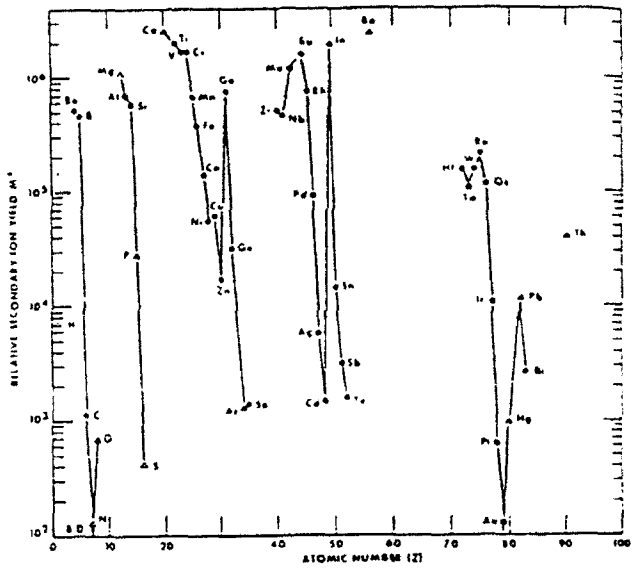

Both these diagrams show magnesium to have a slightly higher secondary ion sputter yield than aluminium.

To predict the relative amounts of magnesium and aluminium present on the surface under different experimental conditions a correction factor must be applied to either the magnesium or aluminium secondary ion signal intensity. Measuring the corrected secondary signal intensities of these two elements will give a better estimation of the quantities of magnesium and aluminium on the surface.

The correction factor for the analysis of the alloys was calculated from the spectra of the 50:50 alloy. The static SIMS spectra of the exposed surface (sub-surface) was recorded. Under the experimental conditions used to analyse the alloys it was found that aluminium had a more intense signal than magnesium. The signal intensity of aluminium was divided by the signal intensity

of Mg^{24} giving a ratio. This ratio was multiplied against all other magnesium signal intensities. The calculation and application of this ratio is shown in appendix 1.

To summarise the static SIMS results obtained at Coleraine a graph (see graph 1) of intensity of Al^{27} signal divided by the sum of the Al^{27} and corrected Mg^{24} signals against percentage of aluminium present in alloy (nominal value). This gives us a cross-section surface analysis of the alloys.

This graph illustrates the relative amounts of aluminium present on the surface with increasing aluminium content in the alloy.

Graph 1 : Cross-section of alloy surface

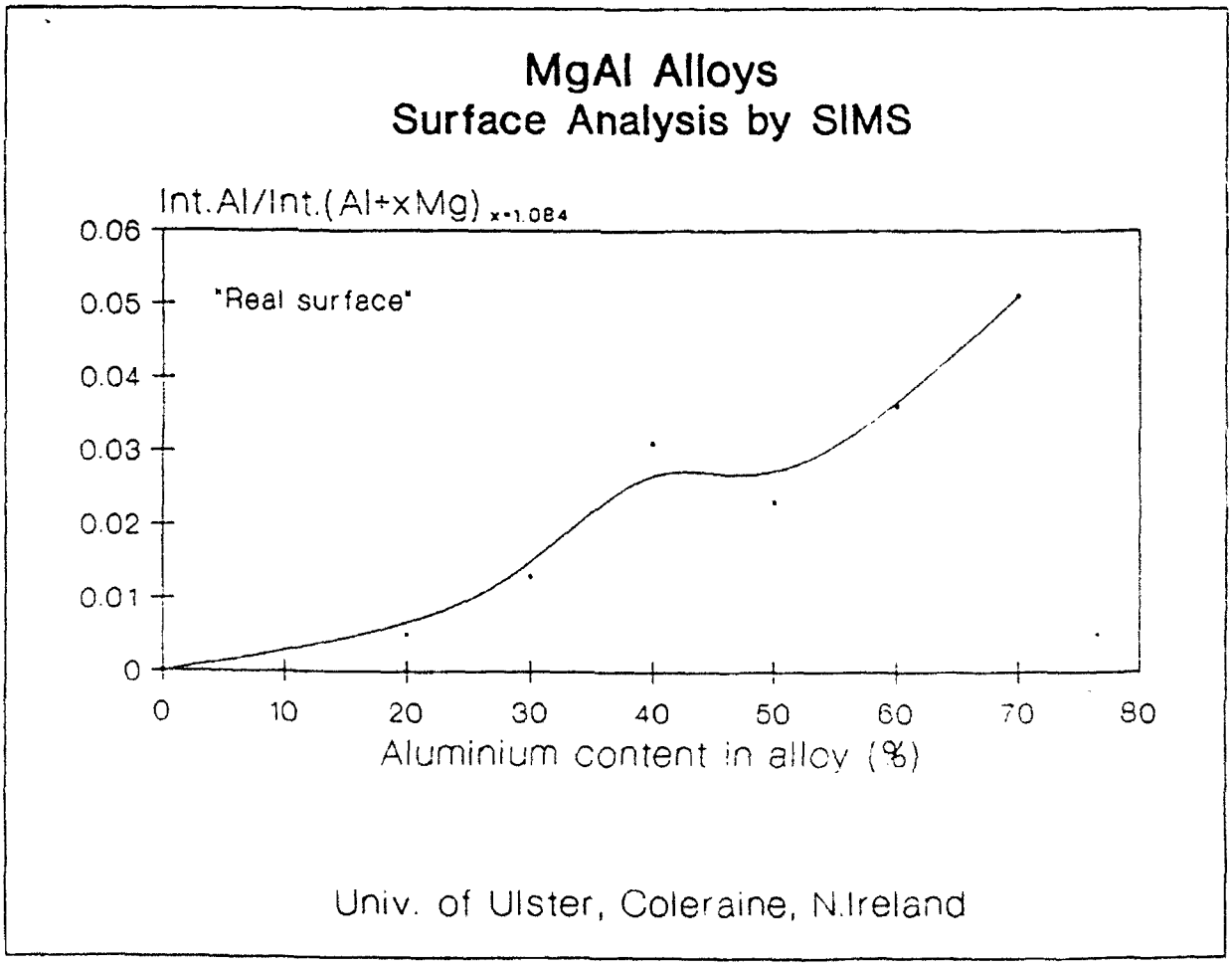

Graph 1 shows increasing amounts of aluminium present on the surface with increasing the amount of aluminium present in the alloy. However, the presence of aluminium on the surface is very small as noted by the low intensity values in the y-axis. The graph also illustrates at 40% aluminium content in alloy a higher aluminium surface content than expected when observing other aluminium values.

4.2 Depth profiles of alloys

The initial part of the profiles show a small signal increase before an 'equilibrium' being reached between impinging and emitting ions. The initial increase at the beginning of the bombardment is the result of the sputter removal of surface contaminents. After an initial rise the signal begins to decrease when the oxide-metal interface is reached and then the signal continues at equilibrium. As mentioned the 'equilibrium' being reached is between the bombardment of O_2^+ ions on the material and the emission of secondary ions. This equilibrium is due to the competing process of O_2^+ ion implantation and sputtering. This process causes the concentration of primary implanted ions at the surface to vary with time, but will finally arrive at a steady-state saturation value when the sputter front has caught up with the implantation front.

Depth profiles of the alloys show that etching further in towards the 'core' of the alloy, the aluminium signal (mass number 27) is strong and steadily rises as we continue etching. This possibly indicates higher amounts of aluminium being exposed as we etch further into the alloy (see pages 36-42).

Observing the three magnesium isotopes (23, 24 and 25), each shows little or no increase in signal intensity thus

indicating an even distribution of magnesium within the alloy particle. Mass number 23, sodium impurity, the signal decreases with further etching into the alloy. The low count rate for sodium indicating very little sodium present, almost negligible. The final mass number detected is 40, representing magnesium oxide. The depth profile indicates, after equilibrium, no increase or decrease in magnesium oxide signal. Ideally, with etching into the alloy, exposing a new surface the magnesium oxide signal would decrease. In this situation we have used a high flux oxygen primary ion gun for depth profile analysis. Here, the high kinetic energy of the incoming oxygen ion is implanting itself within the alloy lattice as well as emitting secondary ions. The oxygen ion implanted from the gun is forming with exposed magnesium particles producing an oxide surface coverage on the exposed surface.

4.3 Static SIMS of exposed surface

Results obtained from the static SIMS analysis of the sub-surface show predominantly aluminium and magnesium to be the two prelevant species on the surface. The high signal intensity of aluminium indicates that the alloys have higher amounts of aluminium within the 'core' of the alloy. In contrast to the initial SIMS analysis of the alloy surface the intensity of the sodium and magnesium oxide signals have decreased. The decrease in the signal

intensity of sodium suggests that the presence of sodium is minute within the 'core' of the alloy and has its highest abundance on the surface of the alloys. The magnesium oxide signal present on the sub-surface is the result of O_2^+ ion implantation on the exposed surface as mentioned in section 4.2.

To summarise the static SIMS results of the sub-surface a graph was plotted (see graph 2) of intensity of Al^{+27} signal

divided by the sum of the Al^{27} and corrected Mg^{24} signals against percentage of aluminium present in alloy (nominal value). This gives us a cross-section surface analysis of the alloy sub-surface.

This graph illustrates the relative amounts of aluminium present on the sub-surface with increasing aluminium content in the alloy.

Graph 2 : Cross-section of alloy sub-surface

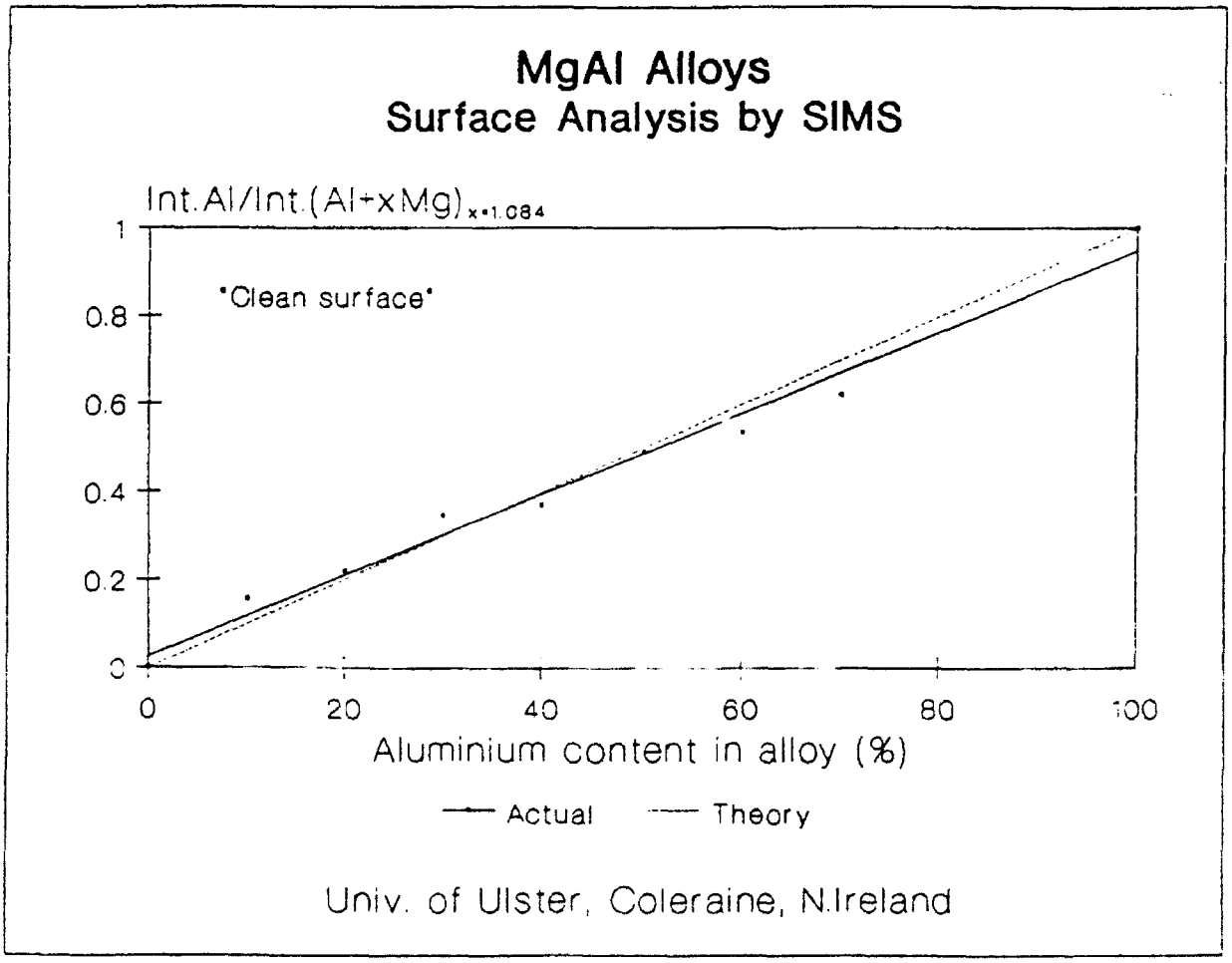

Graph 2 shows that increasing the nominal value of aluminium content in the alloy the amount of aluminium on the sub-surface increases. The points plotted on the graph deviate slightly from the theoretical values. These results indicate that the 'core' of the alloys have more even distributions of magnesium and aluminium than the surface where it is predominantly magnesium.

The intensity ratio on the y-axis of the graph is far greater than that of graph 1. As both static SIMS analysis were performed under identical conditions, the aluminium present on the exposed sub-surface is larger than that of the real surface.

4.4 Rheological analysis of alloys

The results obtained from rheology experiments firstly show that each alloy reacts with the polymer resulting in an increase in viscosity with time (Fig.6). The results indicate that by increasing the nominal amount of magnesium in the alloy there is a greater rate of change of viscosity with time. These results suggest that the presence of aluminium in the alloy has some sort of hinderance effect on the curing reaction. Either, the aluminium has a slower interaction with CTBN than magnesium or, the aluminium does not interact at all with CTBN or, there is some complex manner in which aluminum reacts with CTBN.

Examination of the rheological results of the alloys [Mg:Al 60:40 / Mg:Al 50:50] show that the 50:50 alloy has a higher viscosity than the Mg:Al 60:40 at identical analysis times. This is the inverse of what ideally should happen (the alloy with a greater nominal amount of magnesium will have a faster reaction with CTBN). Both alloys have similar rates of change of viscosity with time. However, surface analysis of both alloys show magnesium to be the prelevant species on the surfaces of the alloys.

Adaptation of the "real" surface analysis results to the cross-section analysis (Graph 1) show that the Mg:Al 60/40 alloy has a higher aluminium surface content than Mg:Al 50/50. This higher aluminium presence could possibly be one reason for the slower reaction indicating aluminium to either interact slower than magnesium or thwarting the reaction in some other manner.

4.5 Surface And Rheology analysis

To connect the surface analysis results to the rheology results two graphs were plotted. Graph 3 shows the viscosity against intensity values of the real surface (i.e. viscosity against Al content on surface).

Graph 3 : Viscosity v's Al content on surface

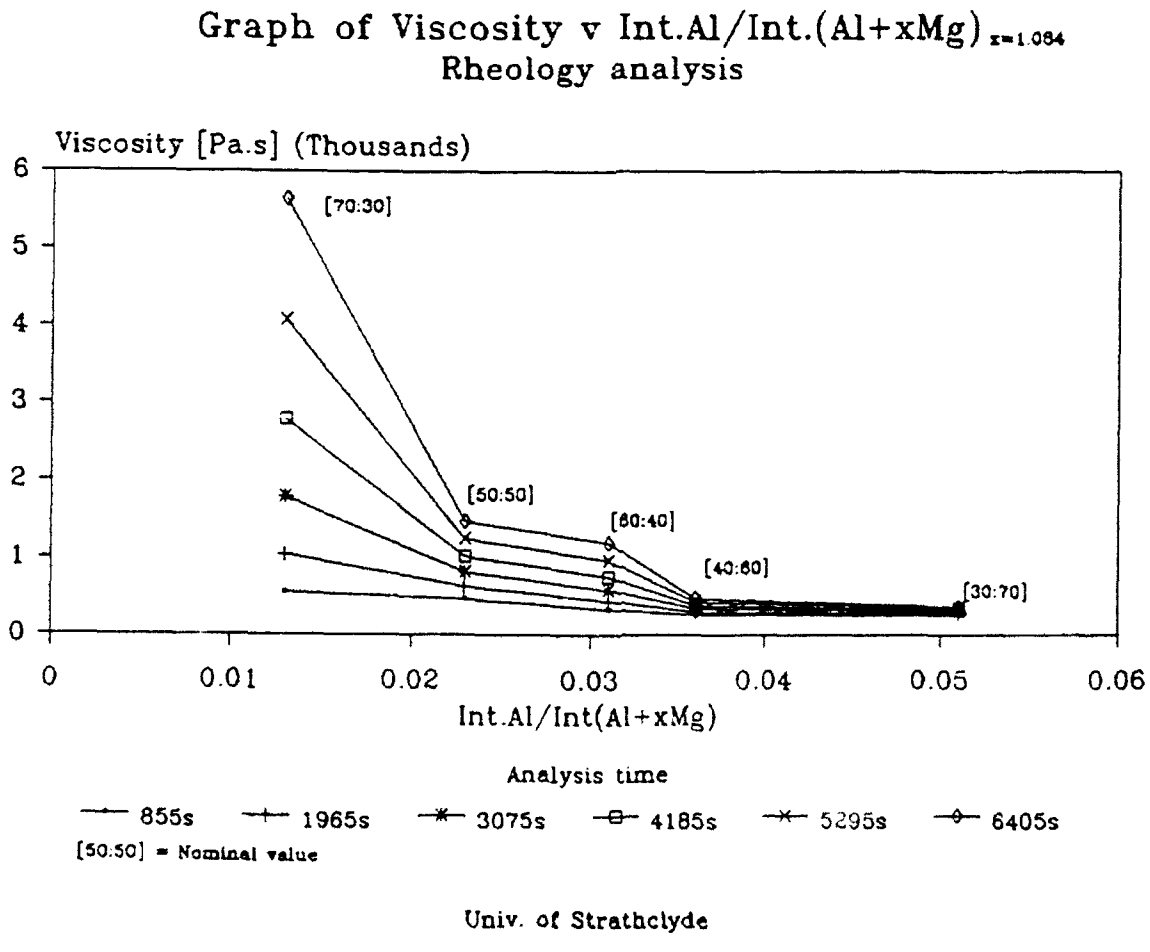

Graph 3 shows with increasing the amount of aluminium surface content the acceleration of the reaction is much slower. As mentioned previously the higher aluminium content for the Mg:Al 60/40 has a slower reaction rate than Mg:Al 50/50 indicating that surface aluminium possibly thwarts the reaction in some complex manner.

Graph 4 is a plot of viscosity against aluminium content on the sub-surface.

Graph 4 : Viscosity v's Al content on sub-surface

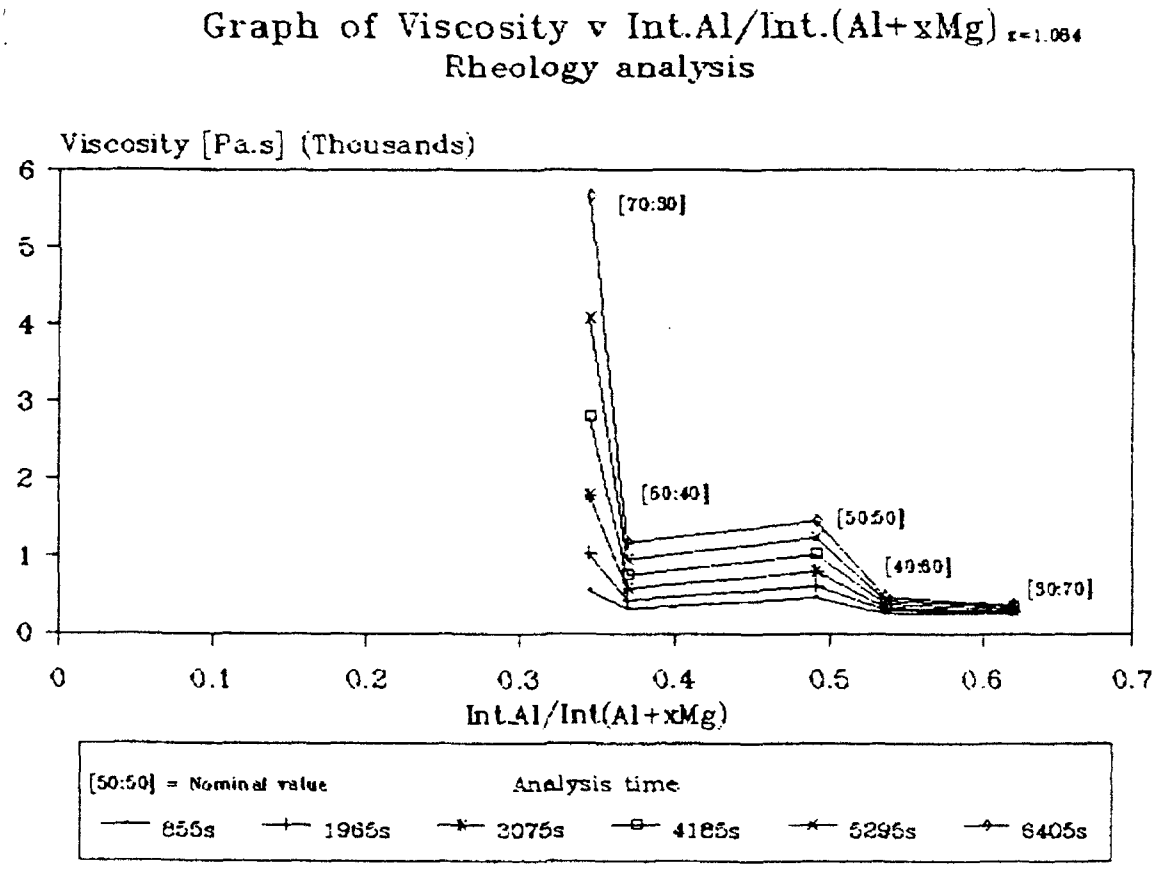

Graph 4 shows the Mg:Al 60/40 alloy to have a lower aluminium content on the sub-surface than Mg:Al 50/50. This results in a slower reaction than Mg:Al 50/50 indicating that a possible complex reaction mechanism is resulting in towards the 'core' of the alloy.

Both graphs 3 and 4 suggest that the interaction of the acid-end groups of CTBN with the alloy surface is that primarily a surface interaction exists which then possibly proceeds to 'eat' through the surface layers of the particle producing another possible surface site for interaction. The reaction seems to proceed in a complex manner.

CHAPTER 5 : FUTURE WORK

For future work we aim to continue, with adsorbing the most effective silanes which were successful in the previous rheology experiments of M^{c}Nab on to our series of alloys and examining them by DRIFTS, SIMS, and XPS. Rheology analysis will then be conducted out on the coated alloys to examine if they have an influence, if any, on the viscosity of the dispersion.

Synthesis of organosilanes with acid functionalities will continue in order to examine their adsorption and viscosity effects as outlined above.

Experiments will be carried out to give adsorption isotherms for each alloy. This will create problems due to the very small surface area of metal powders.

Each alloy will be investigated for its particle size distribution in order to evaluate any viscosity increase due to particle size. In addition, the surface areas of the alloy particles will be carried out by BET.

APPENDIX 1

Calculation of Al/Mg ratio. Calculation made from static SIMS spectra of sub-surface.

$$\text{Ratio} = \frac{\text{(Height of Al peak)}}{\text{(Height of Mg peak)}}$$

Alloy used Mg/Al = 50:50

Height of Al peak = 117.5mm

Height of Mg peak = 108.4mm

$$\text{Ratio} = \frac{117.5}{108.4} = 1.084$$

Application of ratio to Mg^{+} signal intensities.

Sample calculation of Al/Al+XMg value for graph 1.

$$\text{Ratio} = \frac{\text{(Height of Al peak)}}{\text{(Height of Al peak) + (Corrected height of Mg peak)}}$$

Example : Mg/Al = 50:50

Height of Al peak = 3.5mm

Height of Mg peak = 136mm

Corrected height of Mg peak = 147.4mm

$$\text{Value} = \frac{3.5}{3.5 + (1.084*136)} = \frac{3.5}{3.5 + 147.4}$$

$$= \frac{3.5}{150.9} = 0.023$$

REFERENCES

1: J.Coll.Interface Sci. 106, 334 (1985).

2: Appl.Spectrosc. 38(6), 786 (1984).

3: Surf.Sci. 148, 601 (1984).

4: J.Appl.Polym.Sci. 24, 1985 (1979).

5: McNab C., Annual report (unpublished) 1989, Dept. of Pure and Applied Chemistry, Univ. of Strathclyde. Glasgow, G1 1XL. U.K.

6: Affrossman S., Ferguson J., McNab C., Pethrick R.A., 4th INT. Pyrotechnics Congress, Jersey. (1990).

7: J.Catalysis. 107, 295 (1987).

8: J.Catalysis. 105, 445 (1987).

9: J.Catalysis. 22, 219 (1971).

10: Trans.Farad.Soc. 56, 1409 (1960).

11: J.Catalysis. 35, 247 (1974).

12: J.Catalysis. 38, 101 (1975).

13: J.Amer.Chem.Soc. 109, 5197 (1987).

14: J.Chem.Soc.(A). 2784 (1970).

15: J.Catalysis. 7, 67 (1967).

16: J.Catalysis. 104, 299 (1987).

17: Bull.Chem.Soc.Japan. 48, 2527 (1975).

18: Trans.Farad.Soc. 74, 457 (1978).

19: J.Phys.Chem., 64, 1526 (1960).

20: J.Phys.Chem., 69, 220 (1965).

21: Applied Catalysis. 71, 219 (1991).

22: Chem.Abs.(A). 201, 116 (Apr. 1991).

23: J.Amer Chem.Soc. 60, 7 (1938).